

1 **Constraining the timing and processes of pediment formation and**
2 **dissection: implications for long-term evolution in the Western Cape,**
3 **South Africa**

4 Janet C. Richardson¹, Veerle Vanacker², David M. Hodgson³, Marcus Christl⁴, Andreas Lang⁵

5 ¹Geography and Geology: Department of History, Geography and Social Sciences, Edge Hill University, Ormskirk, L39 4QP,
6 UK

7 ²Earth and Life Institute, Centre for Earth and Climate Research, Université catholique de Louvain, Louvain-la-Neuve,
8 1348, Belgium

9 ³School of Earth and Environment, University of Leeds, Leeds, LS2 9JT, UK

10 ⁴Ion Beam Physics, ETH Zürich, Zürich, Otto-Stern-Weg 5, CH 8093, Switzerland

11 ⁵Department of Geography and Geology, Universität Salzburg, Salzburg, A-5020, Austria

12

13 *Correspondence to:* Janet C. Richardson (Janet.Richardson@edgehill.ac.uk)

14 **Abstract.** Pediment surfaces are a widespread feature of the southern African landscape and have long been regarded as ancient
15 landforms. Cosmogenic nuclide data from four pediment surfaces in the Gouritz catchment, Western Cape, South Africa are
16 reported, including boulder surface samples and a depth profile through a colluvial pediment deposit. Pediment surfaces are
17 remarkably stable with long-term denudation rates between 0.3 and 1.0 m My⁻¹, and their ¹⁰Be concentrations approach or at
18 secular equilibrium. Duricrusts have developed in the pediments and are preserved in some locations, which represent an
19 internal geomorphic threshold limiting denudation and indicate at least 2 My of geomorphic stability following pediment
20 formation. The pediments and the neighbouring Cape Fold Belt are deeply dissected by small order streams that form up to
21 280 m deep river valleys in the resistant fold belt bedrock geology, indicating a secondary incision phase of the pediments by
22 these smaller order streams. Using the broader stratigraphic and geomorphic framework, the minimum age of pediment
23 formation is considered to be Miocene. Several pediment surfaces grade above the present trunk valleys of the Gouritz River,
24 which suggests that the trunk rivers are long-lived features that acted as local base levels during pediment formation and later
25 incised pediments to present levels. The geomorphic processes controlling the formation and evolution of the pediments varied
26 over time; with pediments formed by hillslope diffusive processes as shown by the lack of fluvial indicators in the colluvial
27 deposits and later development by fluvial processes with small tributaries dissecting the pediments. Integrating various strands
28 of evidence indicates that the pediments are long-lived features.

29

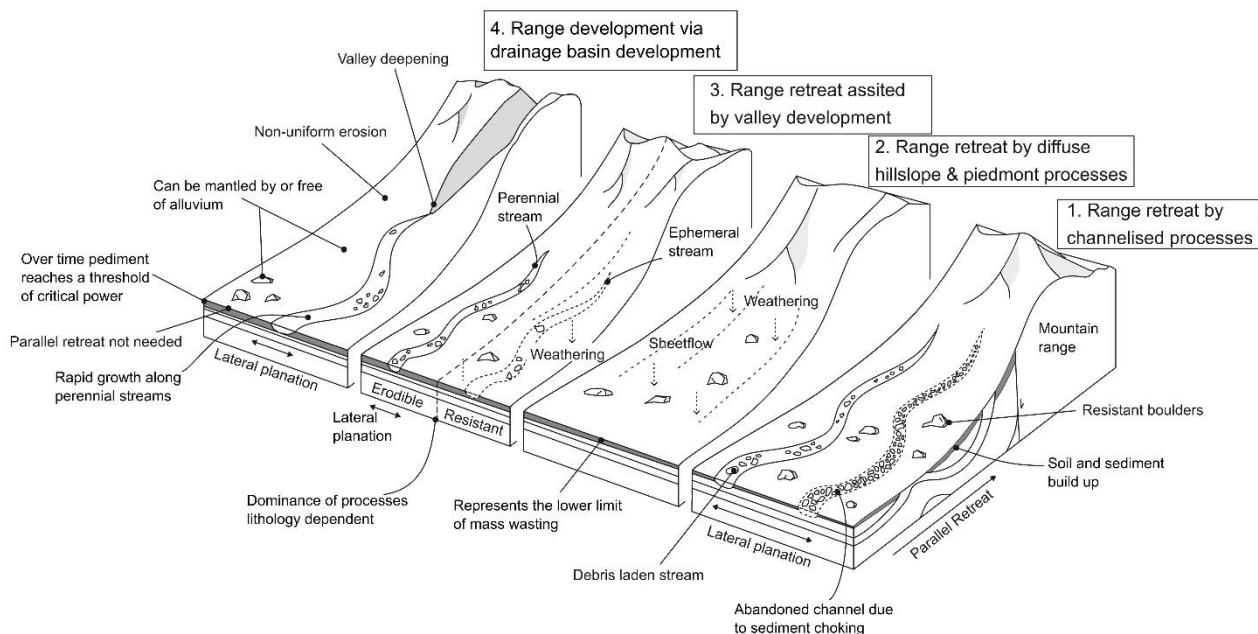
30 **1 Introduction**

31

32 Recent advancements in geochronology allow erosion rates and exposure ages of landforms to be established, and to place
33 more precise constraints on landscape evolution. Establishing erosion rates and landform ages is essential for linking the
34 evolution of drainage systems to downstream aggradation processes (e.g. Gallagher and Brown, 1999; Chappell et al., 2006;
35 Tinker et al., 2008a; Wittmann et al., 2009; Sømme et al., 2011; Romans et al., 2016), constraining surface uplift and tectonic
36 processes (e.g., Brook et al., 1995; Burbank et al., 1996; Granger et al., 1997; Jackson et al., 2002; Wittmann et al., 2007;
37 Bellin et al., 2014; Vanacker et al., 2015), and palaeo-climate reconstructions (e.g., Margerison et al., 2005; Dunai et al., 2005;
38 Owen et al., 2005; Willenbring and Blackenburg, 2010). Reconstructing ancient landforms and landscape development is
39 challenging due to fragmented preservation and increasing signal overprinting forming a landscape palimpsest (e.g. Chorley
40 et al., 1984; Bloom, 2002; Bishop, 2007; Jerolmack and Paola, 2010; Richardson et al., 2016). However, ancient landscapes
41 and landforms cover a large portion of the globe (e.g., (1) Australia – e.g., Ollier, 1991, Ollier and Pain, 2000, Twidale, 2007
42 a,b; (2) southern South Africa – e.g., Du Toit, 1954, King 1956a, (3) South America – e.g. King, 1956b, Carignano et al., 1999,
43 Demoulin et al., 2005, Panario et al., 2014, Peulvast and Bétard, 2015; (4) Asia – e.g., Gorelov et al., 1970, Gunnell et al.,
44 2007, Vanacker et al., 2007; and (5) Europe – e.g., Lidmar-Bergström, 1988, Bessin et al., 2015) and offer important insights
45 into long-term Earth surface dynamics and landscape evolution (indicating variation in erosion and deposition). Further,
46 pediments and planation surfaces can offer insights into mantle dynamics as they are characterised by undulations with middle
47 (several tens of kms) to very long wavelengths (several thousands of kms) characteristic of lithospheric and mantle
48 deformations (e.g., Braun et al., 2014; Guillocheau et al. 2018).

49

50 The formation of pediments is contentious and four categories of landscape evolution models (Fig.1) exist that address the
51 evolution of pediments and surrounding mountain belts (Dohrenward and Parsons, 2009) (1) range front retreat where
52 channelised fluvial processes are dominant (e.g., Gilbert, 1877; Paige, 1912; Howard 1942); (2) range front retreat where
53 diffuse hillslope and piedmont processes are dominant (e.g., Lawson, 1915; Rich; 1935; Kesel, 1977; Bourne and Twidale,
54 1998; Dauteuil et al., 2015); (3) range front retreat as a result of fluvial and diffusive erosion processes (e.g., Bryan, 1923;
55 Sharp, 1940); and (4) lowering of the range due to channelised flow, catchment development and fluvial incision (e.g., Lustig,
56 1969; Parsons and Abrahams, 1984). Model type 1 also acknowledges the occurrence of diffusive processes and model type 2
57 the occurrence of channelised erosion processes, but consider them as subsidiary formation processes (Gilbert, 1877; Rich,
58 1935; Howard, 1942). Model type 3 integrates fluvial and diffusive erosion processes, and their relative importance depends
59 on the geomorphic setting (Bryan, 1923; Sharp, 1940) with a dominance of diffusive processes in regions with erosion-resistant
60 bedrock lithologies, ephemeral streams, and low range. Model type 4 is associated with drainage basin development in the
61 range, and does not require parallel retreat of the mountain front to form the pediment surfaces (Lustig, 1969; Parsons and
62 Abrahams, 1984).



64

65 **Figure 1: Pediment evolution models showing the range of processes that can shape pediments; 1) Range retreat by**
 66 **channelised processes adapted from Gilbert, (1877), Paige (1912) and Howard (1942); 2) Range retreat by diffuse**
 67 **hillslope and piedmont processes adapted from Lawson (1915), Rich (1935), Kesel (1977), Bourne and Twidale (1998)**
 68 **and Dauteuil et al. (2015); 3) Range retreat assisted by valley development adapted from Bryan (1923) and Sharp (1940)**
 69 **and; 4) Range development via drainage basin development adapted from Lustig (1969) and Parsons and Abrahams**
 70 **(1984).**

71

72 The geomorphology of southern Africa has long intrigued earth scientists (Rogers, 1903; Davis, 1906; Dixey, 1944; King,
 73 1948, 1949, 1953). Fundamental questions related to long-term landscape development remain contentious, such as the
 74 mechanisms and timing of surface uplift (e.g., Gallagher and Brown, 1999, Brown et al., 2002, Tinker et al., 2008b, Kounov
 75 et al., 2009, Decker et al., 2013; Wildman et al. 2015; Wildman et al. 2017; Stanley et al. 2021) and the chronological
 76 framework of the main phases of landscape development (Du Toit, 1937, 1954; King, 1951; Burke, 1996; Partridge, 1998;
 77 Brown et al., 2002; Doucouré and de Wit, 2003; de Wit, 2007; Kounov et al., 2015). In-situ produced cosmogenic nuclides
 78 (CRN) can offer key information to unravel questions related to landscape development and evolution and have been applied
 79 to ancient landforms within southern Africa (Fleming et al. 1999; Cockburn et al., 2000; Bierman and Caffee, 2001; van der
 80 Wateren and Dunai, 2001; Kounov et al., 2007; Codilean et al., 2008; Dirks et al., 2010; Decker et al., 2011; Erlanger et al.,
 81 2012; Chadwick et al., 2013; Decker et al., 2013). However, studies based on in-situ produced cosmogenic studies, in the
 82 region south of the Great Escarpment are sparse (e.g., Scharf et al., 2013; Bierman et al., 2014; Kounov et al., 2015).

83

84 Pediments or erosional surfaces have been investigated in South Africa since the 1950's (King, 1953; King 1963; Partridge
85 and Maud, 1987), and have denudation rates that are an order of magnitude lower than those in other landforms within southern
86 Africa (van der Wateren and Dunai, 2001; Bierman et al., 2014; Kounov et al., 2015; Fig. 2). The pediment surfaces were
87 inferred as being early Cenozoic to Jurassic in age by King (1963). Large scale erosional features are also a feature of the
88 wider African continent, and extensive research has been undertaken to understand mantle dynamics associated with plateau
89 formation (e.g., Braun et al., 2014; Dauteuil et al., 2015; Guillocheau et al., 2015; Guillocheau et al., 2018). In this paper, we
90 present new isotopic data from pediment landforms in southern South Africa. The main aim of the paper is to constrain
91 landscape development using in-situ produced ^{10}Be isotopes and to establish denudation rates and landform exposure ages.
92 The objectives of the paper are to: 1) assess the formative process associated with pediment evolution; 2) assess the cosmogenic
93 data within a wider geomorphic and geologic framework in order to test the performance of cosmogenic dating in a geomorphic
94 setting with very low denudation rates; and 3) discuss the implications for the wider landscape development of southern South
95 Africa.

96 **2 Regional Setting**

97 **2.1 Geological setting**

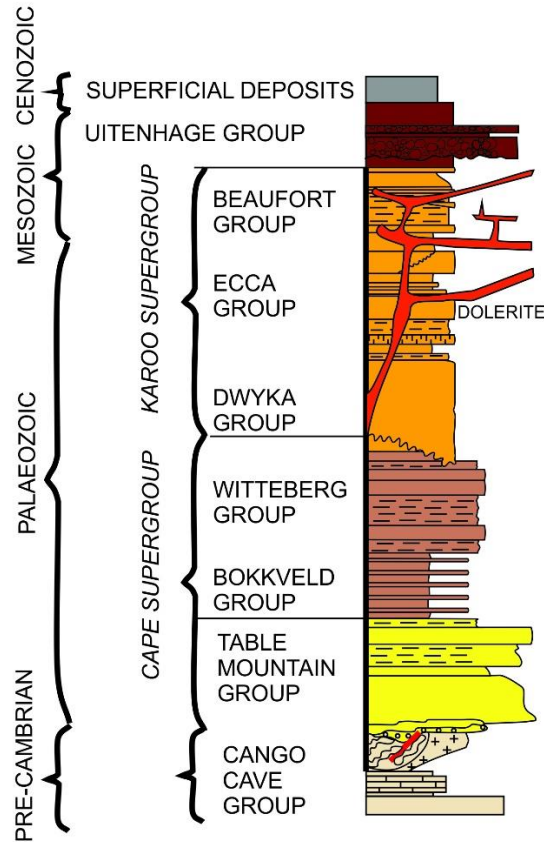
98 In the Western Cape, Southern Africa, the geology is dominated by strata of the Cape (Early Ordovician to Early
99 Carboniferous) and Karoo Supergroups (Late Carboniferous to Early Jurassic) (Johnson et al. 1995, Frimmel et al. 2001) (Fig.
100 2), which are composed of various sandstone, siltstone and mudstone successions. Both supergroups have been subject to low-
101 grade burial metamorphism (Frimmel et al., 2001), with localised contact metamorphism during Jurassic dolerite intrusion
102 (Johnson et al. 1995), and an estimated 6-7 km of exhumation during the Early Cretaceous (Tinker et al., 2008; Wildman et al.,
103 2015). Tectonic shortening during the latest Palaeozoic-to-early Mesozoic of the Cape and Karoo Supergroups of Cape and
104 Karoo Supergroups (Tankard et al. 2009; Hansma et al. 2016) have resulted in with E-W trending, northward verging, and
105 eastward plunging folds that decrease in amplitude northward and shorten northwards, and form the backbone of the exhumed
106 Cape Fold Belt (CFB) (Paton, 2006; Tinker et al., 2008b; Scharf et al., 2013; Spikings et al., 2015). During the Mesozoic, the
107 rifting of Gondwana initiated large-scale denudation across southern Africa. Using apatite fission track analyses of outcrop
108 and borehole samples, Tinker et al. (2008a) concluded that the southern Cape escarpment and coastal plain underwent 3.3 to
109 4.5 km of denudation since the Mid-Late Cretaceous and potentially 1.5 to 4 km within the Early Cretaceous, using a thermal
110 gradient of $\sim 20^\circ\text{C}/\text{km}$. Wildman et al. (2015) processed 75 apatite fission track and 8 zircon fission track data from outcrop
111 and boreholes across the southwestern cape of South Africa (from coast to the escarpment). Using a thermal model and a
112 geothermal gradient of $22^\circ\text{C}/\text{km}$, they obtained an average of 4.5 km denudation in the Mesozoic, from the late Jurassic to the
113 Early Cretaceous. However, their estimates range between 2.2 and 8.8 km of denudation using the upper and lower ranges of
114 the geothermal gradient and possible thermal histories bounded by 95% significance intervals, which provides uncertainty on
115 the inferred exhumation model. Richardson et al. (2017) used reconstructed geological cross sections, tied to apatite fission

116 track data, and drainage reconstruction to model up to 4-11 km of denudation across the Western Cape, with significant
117 exhumation in the Early Cretaceous and lower amounts in the Late Cretaceous.

118

119

120



121

122 **Figure 2: Stratigraphic chart showing the major lithostratigraphic units of the Western Cape, South Africa.**

123

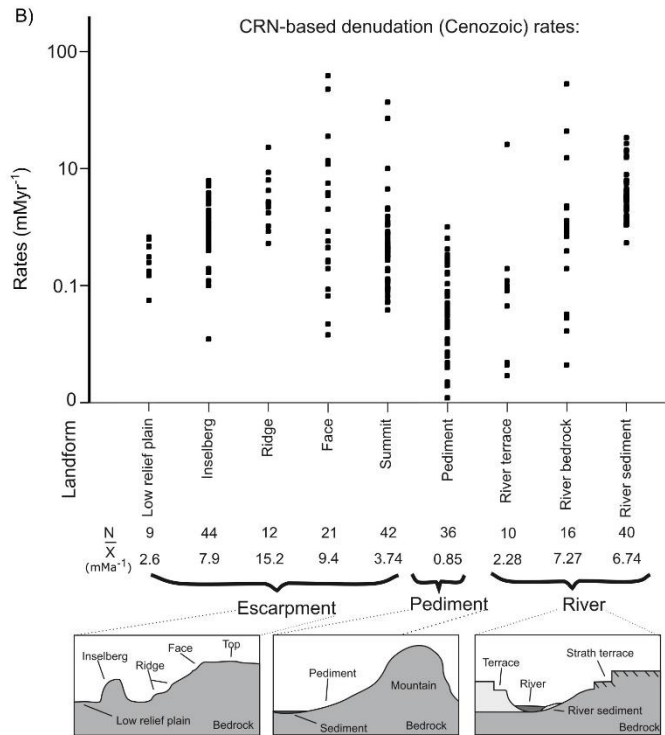
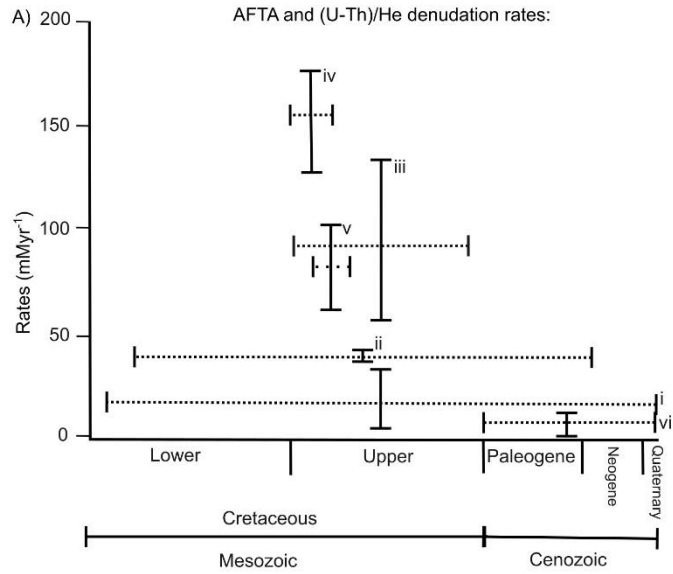
124 The mechanisms of regional uplift during the Mesozoic, related to the anomalous height of southern Africa, are contentious;
125 with landscape evolution either associated to mantle plumes (Nyblade and Robinson, 1994, Ebinger and Sleep, 1998) or to
126 plate tectonics, with uplift along flexures (Moore et al., 2009) resulting in epeirogenic uplift (Brown et al., 1990). Furthermore,
127 the occurrence and timing of later Cenozoic uplift is disputed (e.g., Brown et al., 2002; van der Beek et al., 2002). Burke (1996)
128 proposed that the most recent uplift phase occurred ~30 Ma ago due to a thermal anomaly, and Green et al. (2016) also argued
129 for Cenozoic uplift within southern South Africa that caused localised incision of the Gouritz River into the Swartberg
130 mountain range. Partridge and Maud (1987) argued for two phases of uplift during the Neogene, with a phase around 18 Ma

131 and a more recent phase at 2.58 Ma. Brown et al. (2002) and van der Beek et al. (2002) have questioned Cenozoic uplift based
132 on apatite fission track thermochronology, which does not have a signal for recent uplift.

133

134 Figure 3 provides an overview of published geochronological studies in southern South Africa that used either apatite (U-
135 Th)/He and apatite fission track analysis to document landscape denudation from the Cretaceous to modern day, or in-situ
136 produced cosmogenic radionuclides (^{26}Al , ^{10}Be , ^3He , ^{21}Ne) to date landforms. Apatite (U-Th)/He and fission track data (Fig.
137 3) indicate high rates of denudation (up to 175 m My^{-1} , Tinker et al., 2008b) with respect to the present day rates, towards the
138 end of the Lower Cretaceous (100– 80 Ma) that decreased to up to 95 m My^{-1} by the late Cretaceous (90– 70 Ma; Brown et
139 al., 2002). Flowers and Schoene (2010) report negligible erosion since the Cretaceous, with rates as low as 5 m My^{-1} by the
140 late Eocene (36 My; Cockburn et al., 2000). Cosmogenic studies support low erosion rates within southern South Africa since
141 the start of the Cenozoic (Fig 3; Fleming et al., 1999; Cockburn et al., 2000; Bierman and Caffee, 2001; van der Wateren and
142 Dunai, 2001; Kounov et al., 2007; Codilean et al., 2008; Dirks et al., 2012; Decker et al., 2011; Erlanger et al., 2012; Chadwick
143 et al., 2013; Decker et al., 2013; Scharf et al., 2013; Bierman et al., 2014; Kounov et al., 2015). The majority of landforms are
144 eroding very slowly, with mean denudation rates ranging between 9.4 m My^{-1} for the escarpment faces to 0.85 m My^{-1} for
145 pediments (Fig. 3), although 62.3 m My^{-1} has been measured for one escarpment face retreat (Fleming et al., 1999). In contrast,
146 the Great Escarpment in the South African interior has higher fluvial incision rates than southern South Africa: cosmogenic
147 ^3He channel bed denudation rates range between 14 and 255 m My^{-1} and valley side and valley top denudation rates range
148 between 11 to 50 m My^{-1} for the Klip and Mooi Rivers and Schoonspruit, tributaries of the Orange River (Keen-Zebert et al.,
149 2016).

150



152 **Figure 3: Published exhumation and denudation rates for southern Africa. A) Apatite fission track and (U-Th)/He data**
153 **show large variation in exhumation rates since the Cretaceous, error bars show the range in exhumation rates and**
154 **integration timeframe, and include data from Gallagher and Brown, 1999 (i); Cockburn et al. 2000 (ii); Brown et al.**
155 **2002 (iii); Tinker et al. 2008b (iv); Kounov et al. 2009 (v) and; Flowers and Schoene, 2010 (vi). B) In-situ produced**
156 **cosmogenic (¹⁰Be, ²⁶Al, ²¹Ne and ³He) nuclide-derived denudation rates for escarpment, pediment and fluvial landforms.**
157 **Cosmogenic data is from the following sources; Flemming et al. 1999; Cockburn et al. 2000; Bierman and Caffee, 2001;**
158 **van der Wateren and Dunai, 2001; Kounov et al. 2007; Codilean et al. 2008; Dirks et al. 2012; Decker et al. 2011;**
159 **Erlanger et al. 2012; Chadwick et al. 2013; Decker et al. 2013; Scharf et al. 2013; Bierman et al. 2014; and Kounov et**
160 **al. 2015.**

161

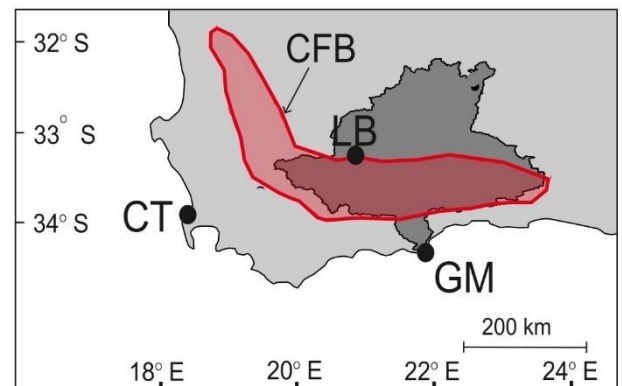
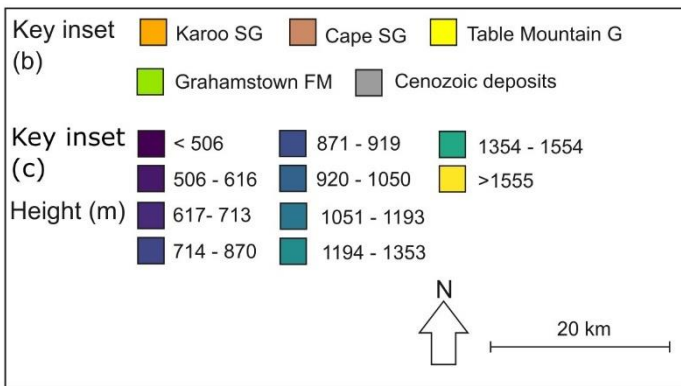
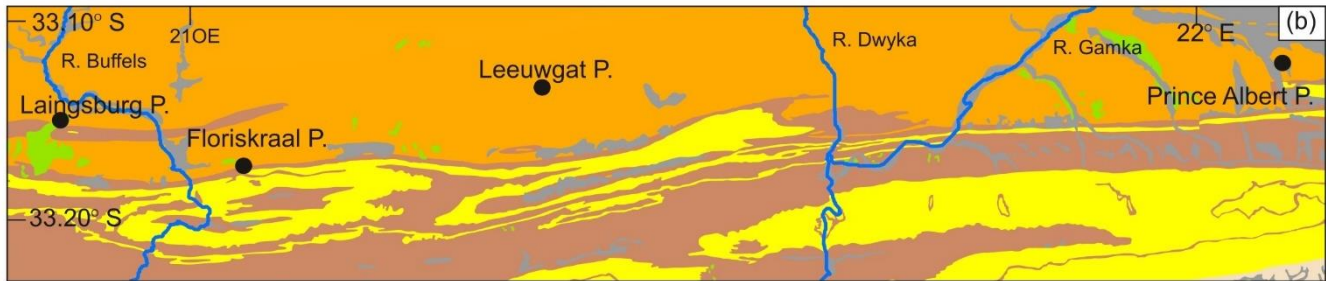
162 Southern South Africa, below the Great Escarpment, is currently tectonically quiescent with only minor Quaternary-active
163 faults (Bierman et al., 2014) and low denudation and sediment production rates (Kounov et al., 2007; Scharf et al. 2013).
164 Minimum exposure ages for pediments range from 0.29 ± 0.02 Ma (Bierman et al., 2014) to 5.18 ± 0.18 Ma (Van der Wateren
165 and Dunai, 2001) with a mean minimum exposure age of 1.87 Ma (Pleistocene, van der Wateren and Dunai, 2001; Bierman et
166 al., 2014; Kounov et al., 2015).

167

168 The climate of southern South Africa has gradually moved towards more arid conditions since the Cretaceous (Partridge, 1997;
169 van Niekerk et al., 1999) with an abrupt change from humid/tropical to arid conditions at the end of the Cretaceous (Partridge
170 and Maud, 2000) as shown by silcrete formation and saline soils (Partridge and Maud, 1987). Although there is general
171 agreement about the overall aridification trend since the Cretaceous, several authors have argued that wetter phases occurred
172 from 65 – 30 Ma (Burke, 1996), or that the arid phase started as late as 18 Ma (Partridge and Maud, 1987). The present-day
173 climate of the Western Cape is primarily semi-arid (Dean et al., 1995), while the coastal region has a Mediterranean type
174 climate (Midgley et al., 2003).

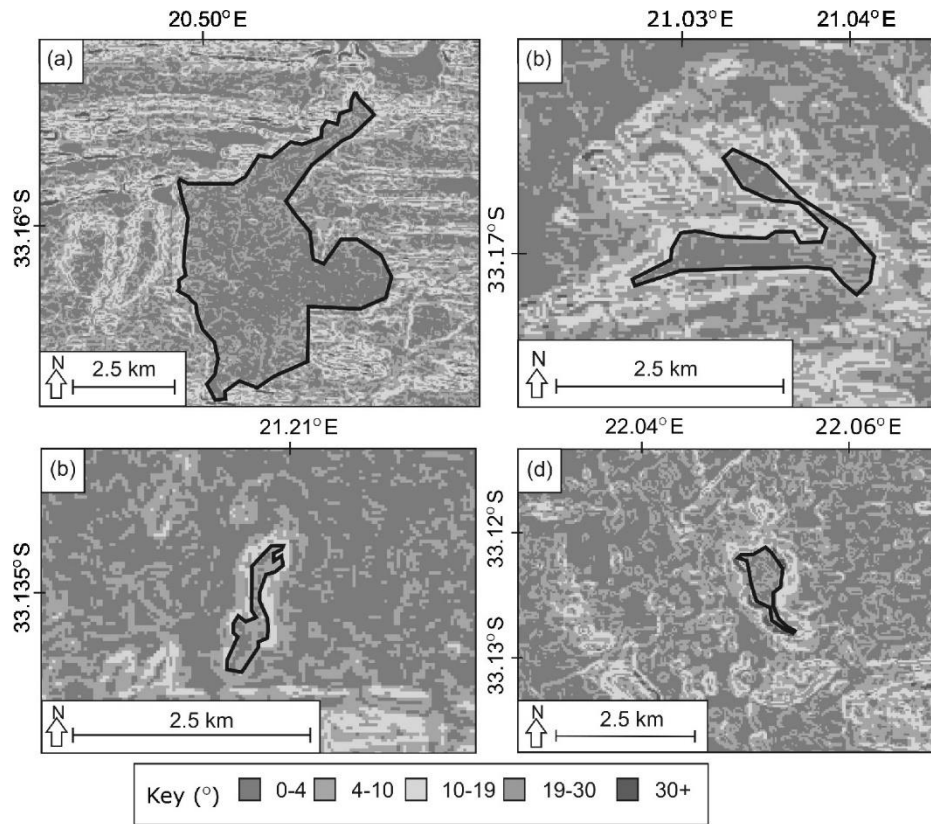
175 **2.2 Sample Sites**

176 The sampling sites are located within the large antecedent Gouritz catchment (Fig. 4), where morphometric analysis has
177 identified the presence of flat surfaces or pediments that carry a thin sedimentary cover, hereafter called alluviated pediments
178 (<1m) (Richardson et al., 2016). The alluviated pediments grade away from the Cape Fold Belt (CFB) into adjacent alluvial
179 plains, and samples were collected from pediments on the northern flank of the Swartberg and Witteberg Mountains (CFB)
180 around Laingsburg, Floriskraal, Leeuwgat, and Prince Albert (Fig. 4a). Samples were taken from five deeply dissected
181 alluviated pediments ranging in surface area between < 1 to 20 km² and displaying slope angles below 10°, with most of the
182 slopes below 4° (Fig. 5).



183

184 **Figure 4: (a) Pediment locations, the inset shows the location of the Gouritz catchment within South Africa, where CT**
 185 **– Cape Town, LB – Laingsburg; GM – Gouritzmond and the red polygon is the location of the Cape Fold Belt (CFB);**
 186 **(b) underlying geology below the pediments and; (c) pediment elevations (in m a.s.l.) as shown by elevation bins**
 187 **categorised by natural breaks in the elevation data. Aerial imagery for (a) from ESRI, Geology information for (b)**
 188 **provided by the Geology Society of South Africa.**



190

191 **Figure 5: Pediment slope data (with slope given in °); (a) Laingsburg; (b) Floriskraal; (c) Leeuwgat and; (e) Prince**
 192 **Albert. For pediment locations please see Figure 4.**

193

194 The alluviated pediments are composed of unconsolidated, poorly-sorted gravel to boulder material in a matrix of sand (Fig.
 195 6) that unconformably overlie folded rocks of the Karoo Supergroup (Fig. 3b). Some pediments are capped by silcrete, calcrete
 196 or ferricrete (Helgren and Butzer, 1977; Summerfield, 1983; Marker and Holmes, 1999; Partridge, 1999; Partridge and Maud,
 197 2000; Marker et al., 2002). Ferricrete is dominant on the Laingsburg pediment. The silcrete is assigned to the Grahamstown
 198 Formation (Fig. 4b) that has poor age control (Mountain, 1980; Summerfield, 1983) due to the lack of formal identification of
 199 the extent of the silcrettes. Electron spin resonance ages for two silcrete caps in the Kleine Karoo were dated at 7.3 and 9.4 Ma
 200 (Hagedorn, 1988).

201



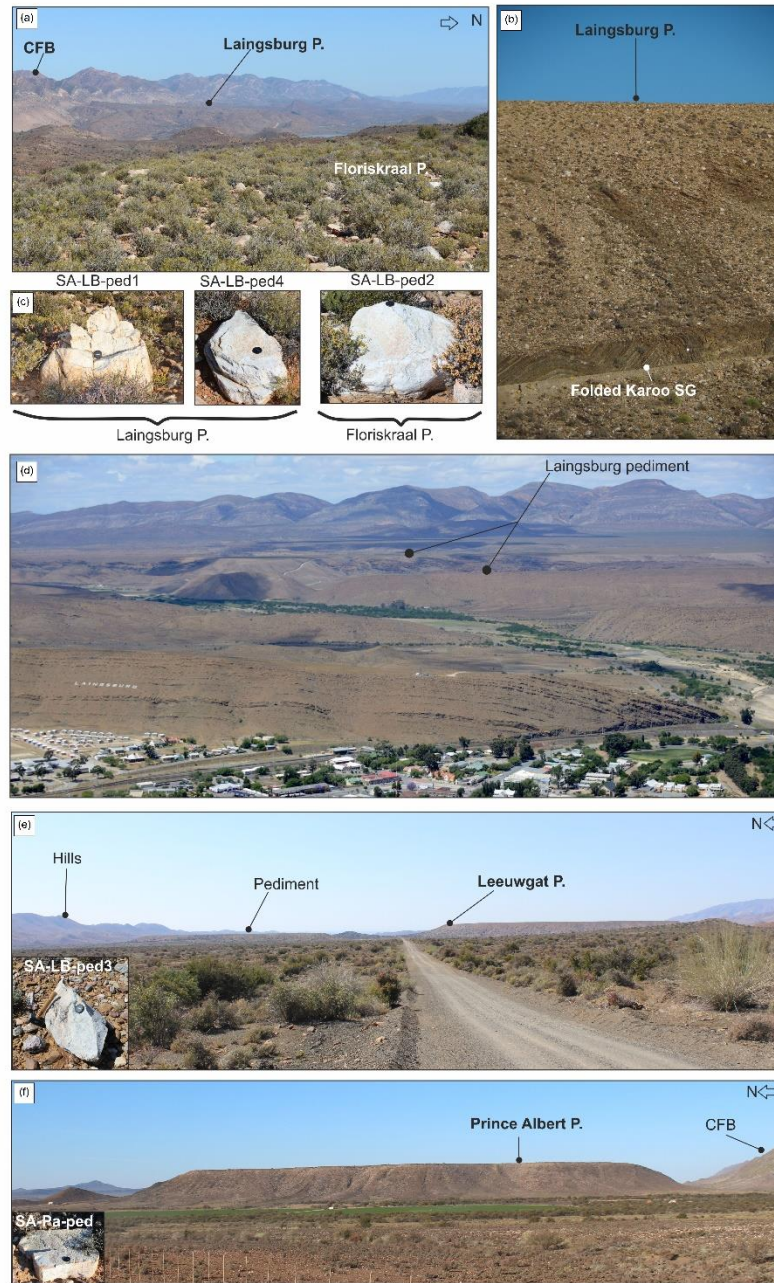
202

203 **Figure 6: (a) Sedimentary log of the Laingsburg pediment showing the unsorted boulders (dominantly quartzite) to**
 204 **gravel size material; (b) photograph of the pediment and where the depth profile clasts were taken; (c) iron-rich**
 205 **palaeosol layer.**

206 3. Methodology

207 3.1 Cosmogenic radionuclide dating

208 Two types of samples were collected for CRN analyses in 2014: five rock samples from alluviated pediment surfaces and
 209 clasts from one depth profile in the Laingsburg pediment (Fig. 7, Table 1). Quartzite boulders from the Table Mountain
 210 Group (Cape Supergroup) that were sampled at the surface of the pediments have a >1m diameter along their longest axis.
 211 For the depth profile in the pediment, quartzite clasts (>25 cm diameter) were taken at the following depths (cm) below
 212 ground level: 0, 30, 85, 150, 255 (Table 1).



213

214 **Figure 7: Sample sites; (a) Laingsburg pediment from the Floriskraal pediment; (b) Laingsburg pediment and**
 215 **contact with underlying folded Karoo Supergroup (SG) strata; (c) Boulder samples from Laingsburg and Floriskraal**
 216 **pediments; (d) large-scale picture of the Laingsburg pediment; (e) Leeuwgat pediment and boulder sample (inset); (f)**
 217 **Prince Albert and boulder sample (inset). The figure also shows the dissection of the pediments by small river**
 218 **catchments and how decoupled the Floriskraal and Prince Albert pediments are from the Cape Fold Belt.**

219 **Table 1: Site-specific information of the sampling sites for cosmogenic radionuclide analysis. All samples are taken**
 220 **from quartzite boulders, that were sampled either on the surface of the pediment (sample type = surf) or at depth**
 221 **(sample type = depth). The density of the sample or overburden (for depth samples) has been determined based on**
 222 **published density data of quartzite boulders and depth profiles in pediments by respectively Scharf et al. (2013) and**
 223 **Kounov et al. (2015).**

Sample ID	Sample type	Name	Latitude (°S)	Longitude (°E)	Elevation (m)	Density (g/cm ³)	Topographic Shielding	Cover correction
SA-PA_ped	Surf	Prince Albert	33.203	22.082	703	2.7	1.00	NA
SA-LB_ped1	Surf	Laingsburg	33.246	20.872	764	2.7	1.00	NA
SA-LB_ped2	Surf	Floriskraal	33.285	21.050	706	2.7	1.00	NA
SA-LB_ped3	Surf	Leeuwgat	33.221	21.347	691	2.7	1.00	NA
SA-LB_ped4	Surf	Laingsburg	33.261	20.854	791	2.7	1.00	NA
SA-LB_DP0	Depth	Laingsburg	33.256	20.851	776	1.6	0.99	NA
SA-LB_DP30	Depth	Laingsburg	33.256	20.851	776	1.6	0.99	0.73
SA-LB_DP85	Depth	Laingsburg	33.256	20.851	776	1.6	0.99	0.41
SA-LB_DP150	Depth	Laingsburg	33.256	20.851	776	1.6	0.99	0.21
SA-LB_DP255	Depth	Laingsburg	33.256	20.851	776	1.6	0.99	0.07

224

225 The samples were processed for in-situ cosmogenic ¹⁰Be following standard methods as described in von Blanckenburg (2004)
 226 and Vanacker et al. (2007). Rock samples were crushed, sieved and rock fragments of 250 to 500 µm diameter were selected
 227 for further lab processing. Quartz minerals were extracted by chemical leaching with a low concentration of acids (HCl, HNO₃,
 228 and HF) in an overhead shaker. Purified quartz samples were then leached with 24% HF for 1h to remove meteoric ¹⁰Be,
 229 followed by spiking the sample with 150 µg of ⁹Be and total decomposition in concentrated HF. The Beryllium in solution
 230 was extracted by ion exchange chromatography as described in von Blanckenburg et al. (1996). The ¹⁰Be/⁹Be ratios were
 231 measured using accelerator mass spectrometer on the 500 kV Tandy facility at ETH Zürich (Christl et al., 2013). Measured
 232 ¹⁰Be/⁹Be ratios were normalised to the ETH in-house secondary standard S2007N with a nominal ratio of 28.1×10⁻¹² (Kubik
 233 and Christl, 2010), which is in agreement with a ¹⁰Be half-life of 1.387 Ma (Chmeleff et al., 2010). Sample ratios were blank
 234 corrected ($7.54 \pm 9.67 \times 10^{-15}$) and the analytical uncertainties on the ¹⁰Be/⁹Be ratios of blanks and samples were then
 235 propagated into the 1σ analytical uncertainty for the ¹⁰Be concentrations (Table 2 and 3). Production rates were scaled
 236 following Dunai (2000) with a sea level high-latitude production rate of 4.28 atoms g_{qtz}⁻¹ yr⁻¹. The bulk density was set to 2.7
 237 g cm⁻³ for samples from quartzite boulders following Scharf et al. (2013), and to 1.6 g cm⁻³ for the overburden of the depth
 238 samples following earlier work on depth profiles in the Western Cape by Kounov et al. (2015). The concentrations were
 239 corrected for topographic shielding using the procedure described in Norton and Vanacker (2009).

240 **Table 2 : Cosmogenic nuclide data for a depth profile in Laingsburg. The reported ^{10}Be concentrations are corrected**
 241 **for procedural blanks, using a value of $7.54 \pm 9.67 \times 10^{-15}$, and the 1σ uncertainty estimates contain analytical errors**
 242 **from AMS measurement and blank error propagation.**
 243

Sample ID	Depth (cm)	^{10}Be concentration ($\pm 1 \sigma$), ($\times 10^6$ at/g _{qtz})
SA-LB_DP0	0	5.460 ± 0.106
SA-LB_DP30	30	1.196 ± 0.111
SA-LB_DP85	85	0.893 ± 0.036
SA-LB_DP150	150	0.376 ± 0.016
SA-LB_DP255	255	0.133 ± 0.015

244

245

246 **Table 3: Cosmogenic nuclide data for surface samples from pediments. The reported ^{10}Be concentrations are corrected**
 247 **for procedural blanks, using a value of $7.54 \pm 9.67 \times 10^{-15}$, and the 1σ uncertainty estimates contain analytical errors**
 248 **from AMS measurement and blank error propagation. Maximum denudation rates and minimum durations of surface**
 249 **exposure were calculated using the CosmoCalc add-in for Excel (Vermeesch, 2007). For the surface exposure ages, we**
 250 **assumed (1) no erosion or burial since exposure, and (2) a maximum steady erosion rate of 0.3 m My^{-1} .**
 251

Sample ID	Location	^{10}Be concentration ($\times 10^6$ at/g _{qtz}) ($\pm 1\sigma$)	^{10}Be denudation rate (m My^{-1}) ($\pm 1\sigma$)	Minimum exposure age (Ma) ($\pm 1\sigma$)	
				No erosion or deposition	Erosion rate of 0.30 m My^{-1}
SA-PA_ped	Prince Albert	2.834 ± 0.055	0.954 ± 0.025	0.569 ± 0.010	0.678 ± 0.010
SA-LB_ped1	Laingsburg	5.199 ± 0.096	0.408 ± 0.013	1.131 ± 0.016	1.964 ± 0.016
SA-LB_ped2	Floriskraal	5.148 ± 0.095	0.383 ± 0.013	1.189 ± 0.016	2.220 ± 0.016
SA-LB_ped3	Leeuwgat	5.641 ± 0.103	0.315 ± 0.011	1.377 ± 0.018	4.462 ± 0.018
SA-LB_ped4	Laingsburg	4.252 ± 0.067	0.587 ± 0.014	0.848 ± 0.011	1.164 ± 0.010
SA-LB_DP0	Laingsburg	5.460 ± 0.106	0.373 ± 0.013	1.210 ± 0.018	2.333 ± 0.018

252

253

254 For the derivation of the minimum durations of exposure (Table 3), we used two different scenarios: a hypothetical case
 255 assuming no erosion or burial since exposure, and a second case assuming steady erosion of the pediment surface of 0.3 m My^{-1}

256 ¹ following Bierman et al. (2014). The CosmoCalc method, version 3.0 (Vermeesch, 2007) was employed to calculate
 257 maximum denudation rates and minimum surface exposure ages from the ¹⁰Be concentrations of the surface samples (Table
 258 3). The surface exposure ages are *minimum estimates* as isotopic steady state can be reached for old material.

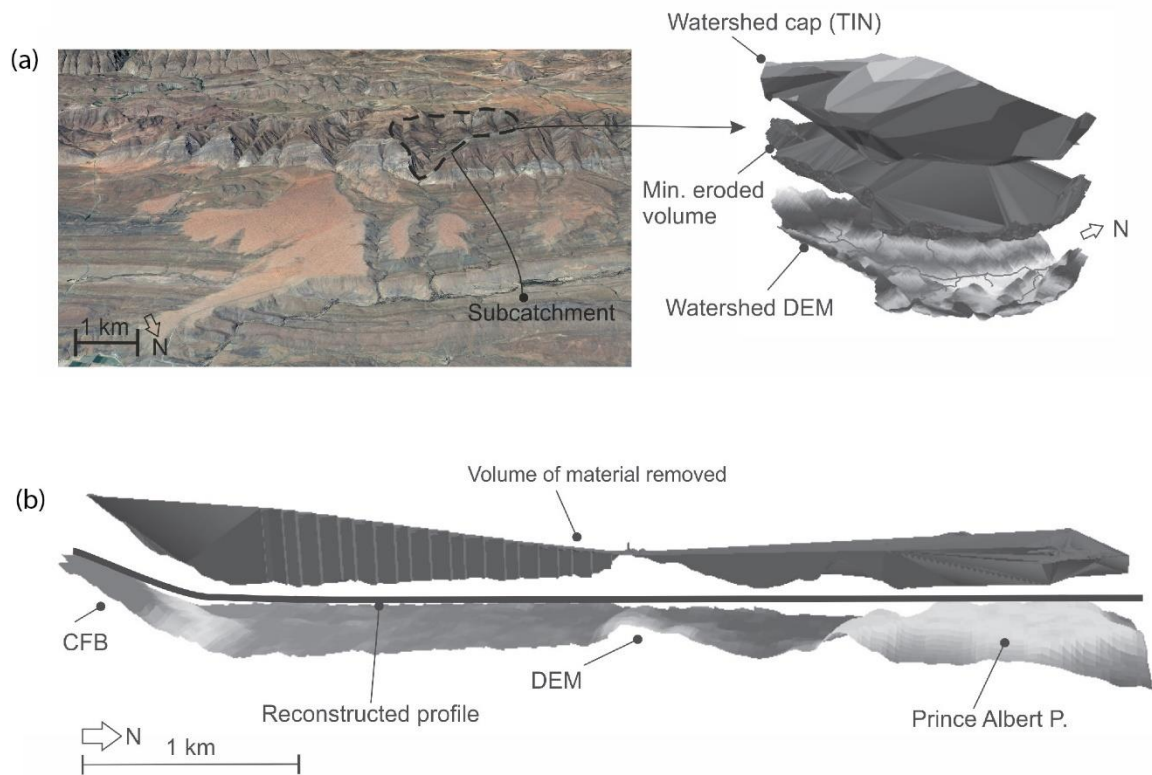
259 In addition, we use a concentration depth profiling approach to better constrain the exposure and denudation of the Laingsburg
 260 area pediment. The accumulation of ¹⁰Be, $N_{\text{total}}(z,t)$, in the eroding surface of the pediments can be described as:

$$261 \quad N(z, t) = N_{\text{inh}}e^{-\lambda t} + \sum_i \frac{P_i(z)}{\lambda + \frac{\rho E}{\Lambda_i}} e^{-\rho(z_0 - Et)/\Lambda_i} \left(1 - e^{-\left(\lambda + \frac{\rho E}{\Lambda_i}\right)t} \right) \quad \text{Eq.1}$$

262 where E is expressed in cm/yr ($\text{m My}^{-1} \times 10^4$), t [y] is the exposure age, λ [y^{-1}] the nuclide decay constant ($\lambda = \ln 2 / t_{1/2}$), z_0
 263 (cm) the initial shielding depth ($z_0 = E \times t$), ρ [g cm^{-3}] the density of the overlying material, and Λ_i [g/cm^2] the attenuation
 264 length. The production rate, $P_i(z)$ [$\text{atoms g}_{\text{qtz}}^{-1}\text{y}^{-1}$], is a function of the depth, z [cm], below the surface. The subscript ‘i’
 265 indicates the different production pathways of ¹⁰Be via spallation, muon capture and fast muons following Dunai (2010). In
 266 this study, the relative spallogenic and muogenic production rates are based on the empirical muogenic-to-spallogenic
 267 production ratios established by Braucher et al. (2011), using a fast muon relative production rate at SLHL of 0.87% and slow
 268 muon relative production rate at SLHL of 0.27%. The attenuation length was set to 152, 1500 and 4320 g cm^{-2} for the
 269 production by, respectively, neutrons, negative muons and fast muons (Braucher et al., 2011). The depth profile is then solved
 270 numerically, based on model fitting between the observed (Table 2) and simulated ¹⁰Be concentrations at different depths, for
 271 a wide range of exposure age (0.4 to 20 Ma), denudation rate (0 to 1.5 m My^{-1}), inheritance ($N_{\text{inh}}e^{-\lambda t} = N_{255\text{cm}}$ vs. no
 272 inheritance) and deflation scenarios. The Nash-Sutcliffe efficiency and the chi-squared were used to assess the predictive
 273 power of the numerical models following Vandermaelen et al. (2022).

274 **3.2 Morphometric Analysis**

275 Aster 30m data was used to build a DEM of the study area in ArcGIS 10.1. The DEM was re-projected into WGS 1984 world
 276 Mercator coordinates and gaps were filled using the hydrology toolbox. The drainage was extracted using an upstream
 277 contributing area of 3.35 km^2 , and both ephemeral and perennial streams were delineated (e.g., Abadelkaarem et al., 2012;
 278 Ghosh et al., 2014). Dissected pediments were derived using a method adapted from Bellin et al. (2014). The previous grading
 279 from the mountain front was reconstructed for each pediment in ArcGIS (Fig. 8). This surface was then placed into ArcScene
 280 10.1, with the difference between the reconstructed surface and the current topography (using the DEM) providing a minimum
 281 volume of material removed after pediment formation. A similar approach was applied to derive bulk erosion volumes for the
 282 small sub-catchments that back the pediment surfaces in the CFB. The bulk erosion is likely to be a minimum estimate of the
 283 total rock volume removed by erosion, as interfluvial erosion might have occurred (Bellin et al., 2014; Brocklehurst and
 284 Whipple, 2002). Eroded volumes were then converted to lithological thickness using the method of Aguilar et al. (2011).



285

286 **Figure 8: Examples of (a) bulk eroded volumes from subcatchments and (b) cross section of the Prince Albert**
 287 **pediment showing the method used in ArcGIS for the volume of material removed around the pediment surface.**
 288 **Imagery for (a) from © Google Earth 2015.**

289 4. Results

290 4.1 Alluviated pediment composition

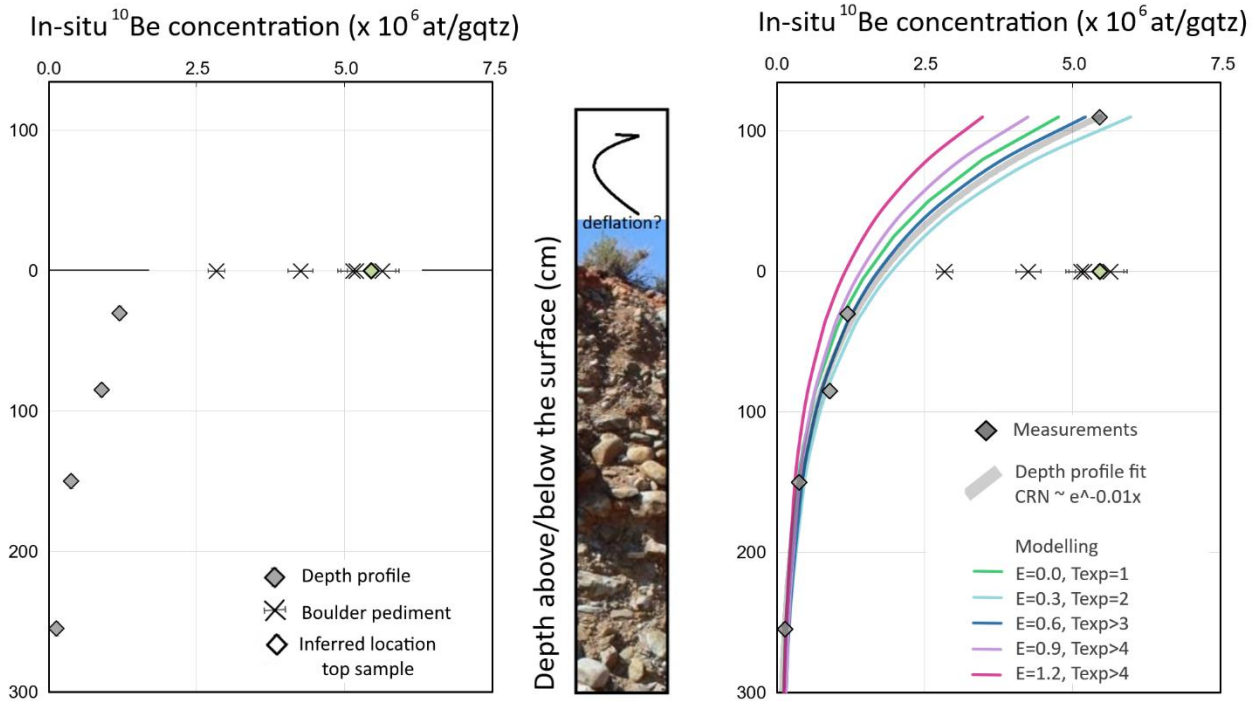
291 The contact with the underlying bedrock (e.g., Dwyka Group) is erosional and undulating, it is not a smooth planation contact.
 292 The alluviated pediments are composed of poorly sorted boulders to pebbles, with a matrix of sandy gravel. The clasts are
 293 predominantly quartzites (Table Mountain Group); however smaller clasts of Dwyka Group lithologies are present. Towards
 294 the top of the profile there is a small transition zone of gravel, which is capped by an iron crust (Fig. 6). There is no indication
 295 of fluvial activity (i.e., imbrication). There is no grading or sediment clast size variation throughout the profile, and the clasts
 296 range from sub-rounded to sub-angular.
 297

298 4.2 Cosmogenic nuclides

299 The in-situ produced ^{10}Be concentrations in boulders sampled on the pediment surface range between $(2.834 \pm 0.055) \times 10^6$
300 and $(5.641 \pm 0.103) \times 10^6$ at/g_{qtz}. The CRN concentrations are indicative for old surfaces with very low denudation, and we
301 obtained long-term denudation rates of 0.315 to 0.954 m My⁻¹ for the pediments. The alluviated pediment in the Prince Albert
302 area has the highest rate of maximum surface lowering (0.954 m My⁻¹), which is an order of magnitude higher than the average
303 surface lowering rate of the pediments in the Laingsburg area. In the latter area, the surface denudation rates decrease from the
304 CFB towards the proximal part of the pediment (Table 3).

305 The alluviated pediments are long-lived, and have been exposed for at least 0.678 to 4.461 My (when we assume that the
306 surface was lowered by 0.3 m My⁻¹). The CRN-depth profile in the Laingsburg pediment demonstrates the existence of a
307 deflation surface as result of differential erosion. The profile consists of 5 samples, taken at the surface, 30, 80, 150 and 255
308 cm depth. The ^{10}Be concentrations steadily decrease with depth (Fig. 9a) whereby the ^{10}Be concentration of four lower samples
309 decreases exponentially with depth, as theoretically expected for cosmogenic radionuclide production by neutrons with a fitted
310 exponent of -0.01 ($N_{^{10}\text{Be}} \approx e^{-0.01 \times \text{depth}}$, RMSE = 1.49×10^5 at/g_{qtz}) corresponding well to an attenuation length of 160 g/cm²
311 for a matrix density of 1.6 g/cm³. In contrast, the top sample (SA-LB-DP0) has a concentration that is more than double the
312 theoretically expected ^{10}Be concentration (Table 3). We attribute this phenomenon to surface deflation: boulders covering the
313 ground surface are part of a deflation armouring, and are longer exposed to cosmic rays than the matrix of sandy gravel in
314 which they are now embedded. Based on the exponential fit through the four lowermost data points, we estimate that ~110 cm
315 of fine-grained matrix was removed from the top of the pediment by deflation (Fig. 9b) resulting in a pavement of old boulders
316 at the top of a slowly eroding surface (Fig. 10).

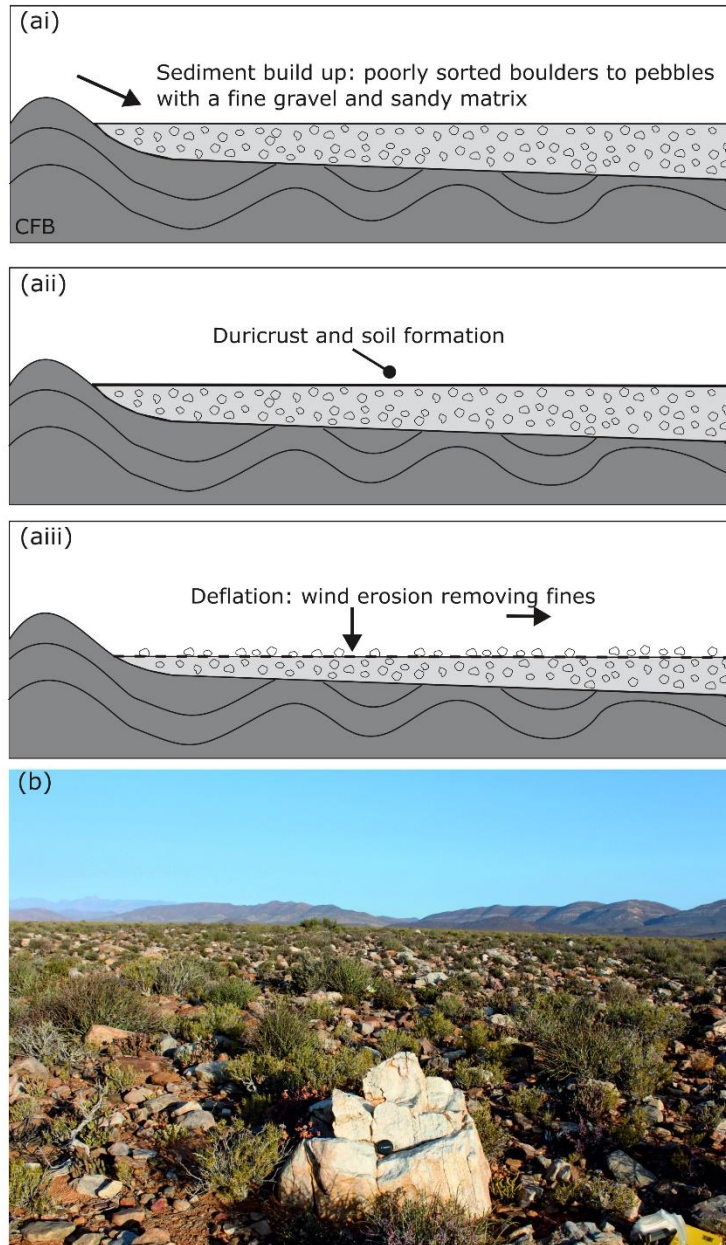
317 ~~The ^{10}Be concentration depth profile provides more insights in the denudation process of the pediments. First, the uppermost~~
318 ~~sample of the Laingsburg depth profile has a ^{10}Be concentration that is in line with the concentrations that are measured in~~
319 ~~boulders sampled at the Laingsburg, Floriskraal and Leeuwgat alluviated pediments, and is markedly higher than the~~
320 ~~concentration measured at the Prince Albert alluviated pediment (Fig. 9a, Table 3). Second, there is a large discrepancy in the~~
321 ~~^{10}Be concentrations between the uppermost sample and the four samples taken at depth in the profile (Table 2). The $4.265 \times$~~
322 ~~10^6 at./g difference in ^{10}Be concentrations over a 30 cm depth increment cannot be explained by steady erosion of the pediment~~
323 ~~after exposure (Fig. 9b). It suggests that deflation of ~110 cm of fine grained material at the surface of the pediments has.~~



324

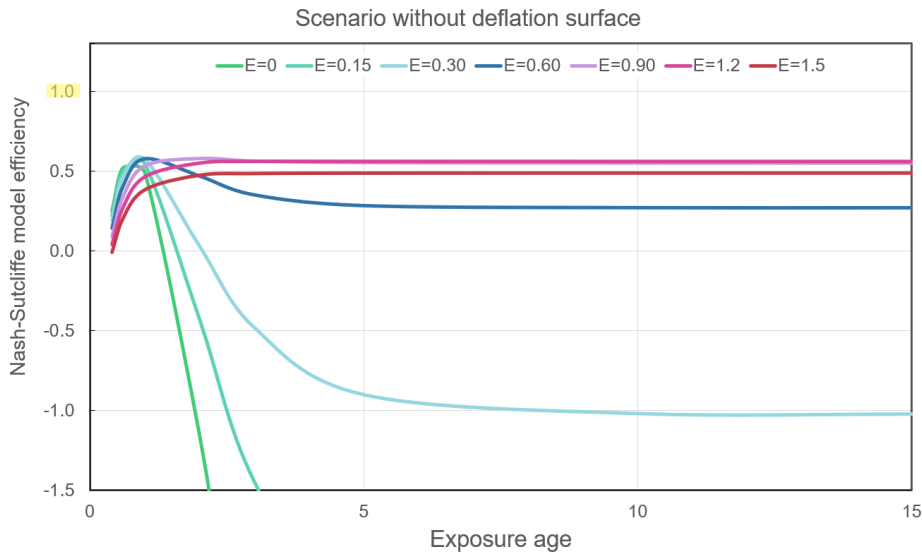
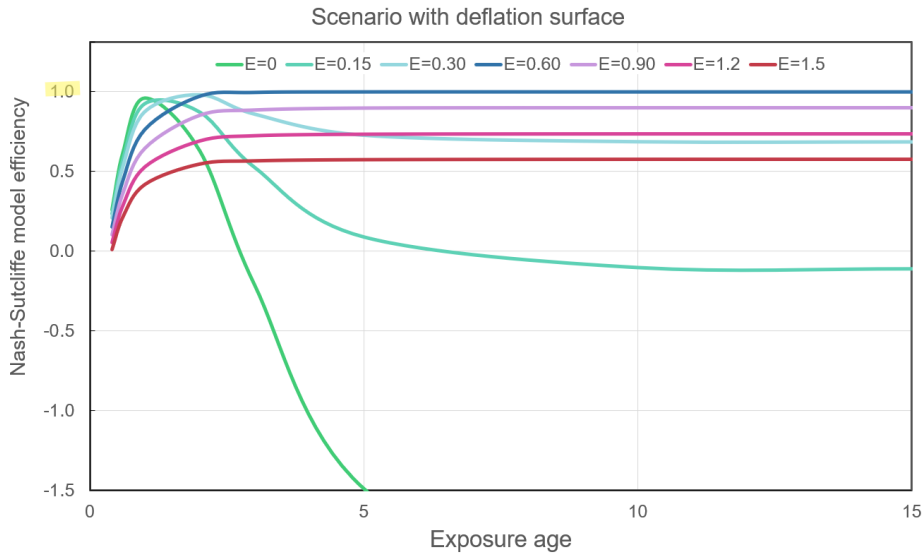
325 **Figure 9: Depth profile in the Laingsburg pediment. (a) showing in-situ ^{10}Be concentrations (expressed in atoms of**
 326 **^{10}Be per g of quartz) as measured in depth profile and boulders from other pediments listed in Table 3, (b) modelled**
 327 **in-situ ^{10}Be concentration from a data-fitted exponential model ($N_{10\text{Be}} \approx e^{-0.01 \times \text{depth}}$) and from numerical**
 328 **simulations using forward modelling for given erosion rates (E expressed in m My^{-1}) and exposure ages (Texp**
 329 **expressed in Ma). For erosion rates exceeding 0.6 m My^{-1} , the in-situ ^{10}Be concentrations are in secular equilibrium**
 330 **for exposure ages exceeding the Texp indicated in the graph, and the concentration-depth profiles become time-**
 331 **invariant.**

332



333

334 **Figure 10: (a) Process of deflation and (b) Evidence of deflation: concentrations of boulders and pebbles on top of the**
 335 **Laingsburg Pediment.**



336

337 **Figure 11: Goodness-of-fit of the model predictions for the ^{10}Be depth concentration profile in the Laingsburg**
 338 **pediment, as evaluated by the Nash-Sutcliffe efficiency (NSE). The NSE ranges between $-\infty$ and 1, whereby 1**
 339 **corresponds to a perfect model fit. Model simulations were realised for a wide range of exposure ages (0 to 20 Ma)**
 340 **and denudation rates ($E = 0$ to 1.5 m My^{-1}), and for conditions with/without inheritance ($N_{inh} e^{-\lambda t} = N_{255\text{cm}}$) and**
 341 **deflation armoring. For simulations with development of armoring, optimal solutions (NSE $\rightarrow 1$) are found for**
 342 **denudation between 0.3 and 0.6 m My^{-1} and exposure ages exceeding 2 Ma . Model performances for simulations**
 343 **neglecting surface deflation are significantly lower (NSE $\rightarrow 0.6$), illustrating the necessity to account for deflation**
 344 **armoring.**

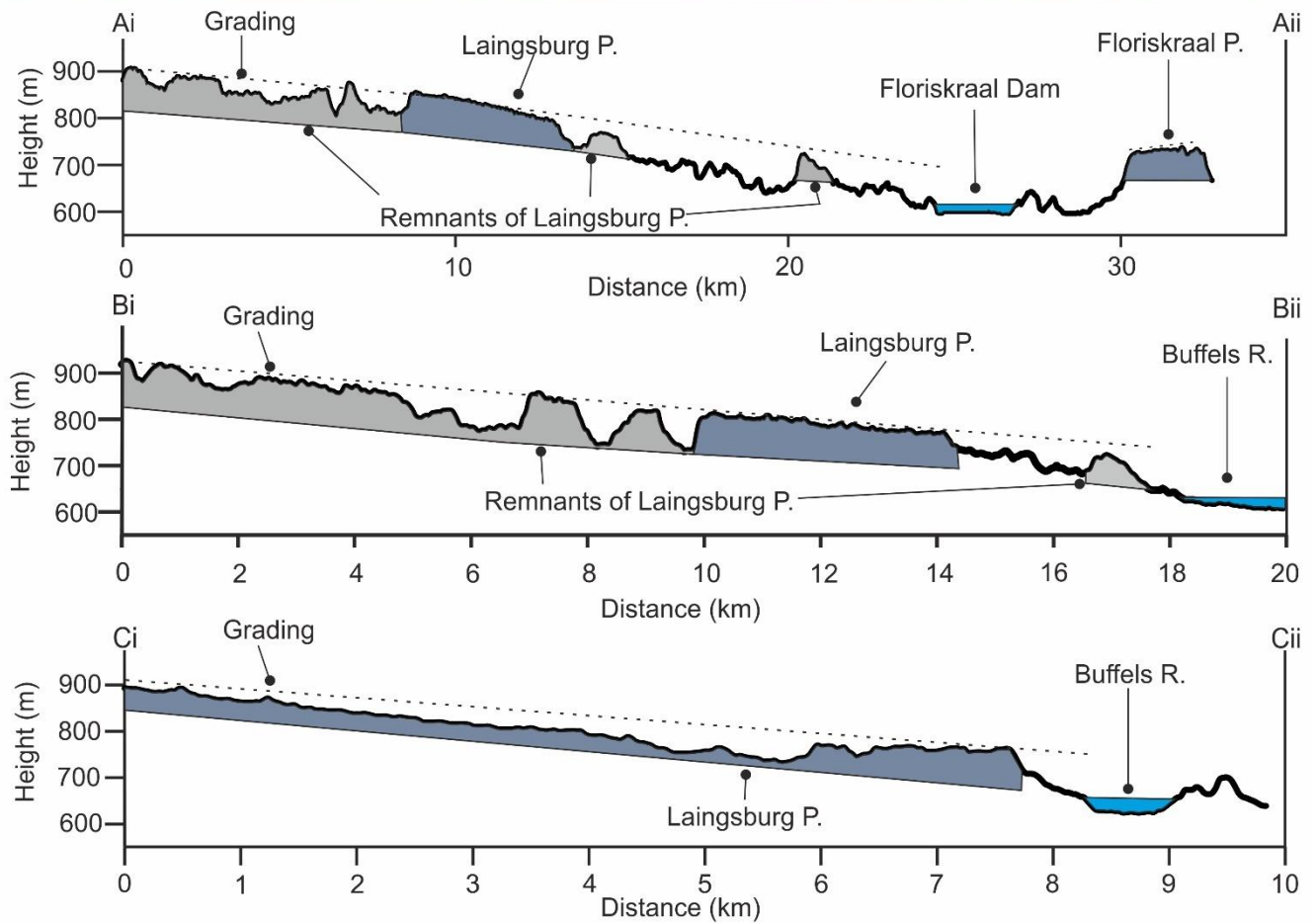
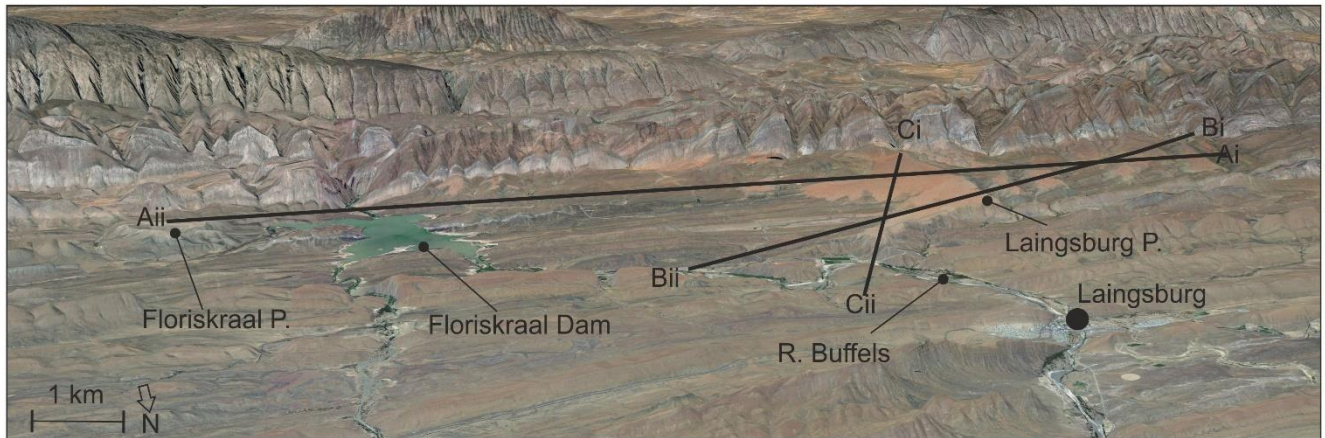
345

348 Based on Eq. 1, we modelled the ^{10}Be concentration depth profile of the Laingsburg pediment for a wide spectrum of possible
349 erosion-exposure age scenarios. We evaluated the goodness-of-fit of the predicted models based on the Nash-Sutcliffe
350 efficiency (NSE) and chi-squared (Fig. 11). Our results show no significant improvement in model performance when
351 accounting for inheritance, indicating that inheritance can be neglected in the analyses of the ^{10}Be depth profiles in the
352 Laingsburg pediment. Otherwise, deflation of the surface is confirmed by the simulation outcomes because (i) model
353 predictions using erosion-exposure age scenarios that disregard deflation all have an NSE below 0.60 while their corresponding
354 scenarios accounting for deflation armouring have an NSE up to 1.00, and (ii) a two-sample comparison t-test confirms
355 significantly lower fit for model predictions that disregard deflation.

356 Optimal model fits, defined as model predictions with an NSE approaching '1' and minimal chi-squared value, are obtained
357 for the scenarios with long-term erosion between 0.3 and 0.6 m My^{-1} , and exposure exceeding 2 Ma. Not only is this result
358 congruent with the outcomes of the CosmoCalc method (Table 3), it also provides more details on the erosion-exposure
359 scenarios that are most likely to explain the long-term evolution of the pediment.

360 **4.3 Elevations and grading of pediment**

361 Figure 4c shows the pediment heights as classified by the Jenks natural break scheme (De Smith and Goodchild, 2007). The
362 alluviated pediments at Laingsburg and Floriskraal have elevations within the same class (714 – 870 m), and the Leeuwgat
363 and Prince Albert area alluviated pediments share the same elevation class (617 – 713 m). The Laingsburg area alluviated
364 pediment appears to have an aspect of slope that grades not only away from the CFB but towards the modern Buffels River
365 location, which abuts the northern limit of the alluviated pediment (Fig. 12). This relationship is less clear on the Floriskraal
366 alluviated pediment, which is to the east of the Buffels River. The alluviated pediment at Leeuwgat, which sits between two
367 folds of the CFB, has no large trunk river nearby (~30 km from Dwyka River) and simply grades away from the CFB (Fig.
368 13a). The Prince Albert area pediment grades towards the Gamka River, although it is currently ~16 km from the Gamka River
369 (Fig. 13b). The fact that the alluviated pediments grade towards the present day trunk rivers but above their present day
370 elevation indicates that these rivers were active during the formation of the pediments and is discussed later.

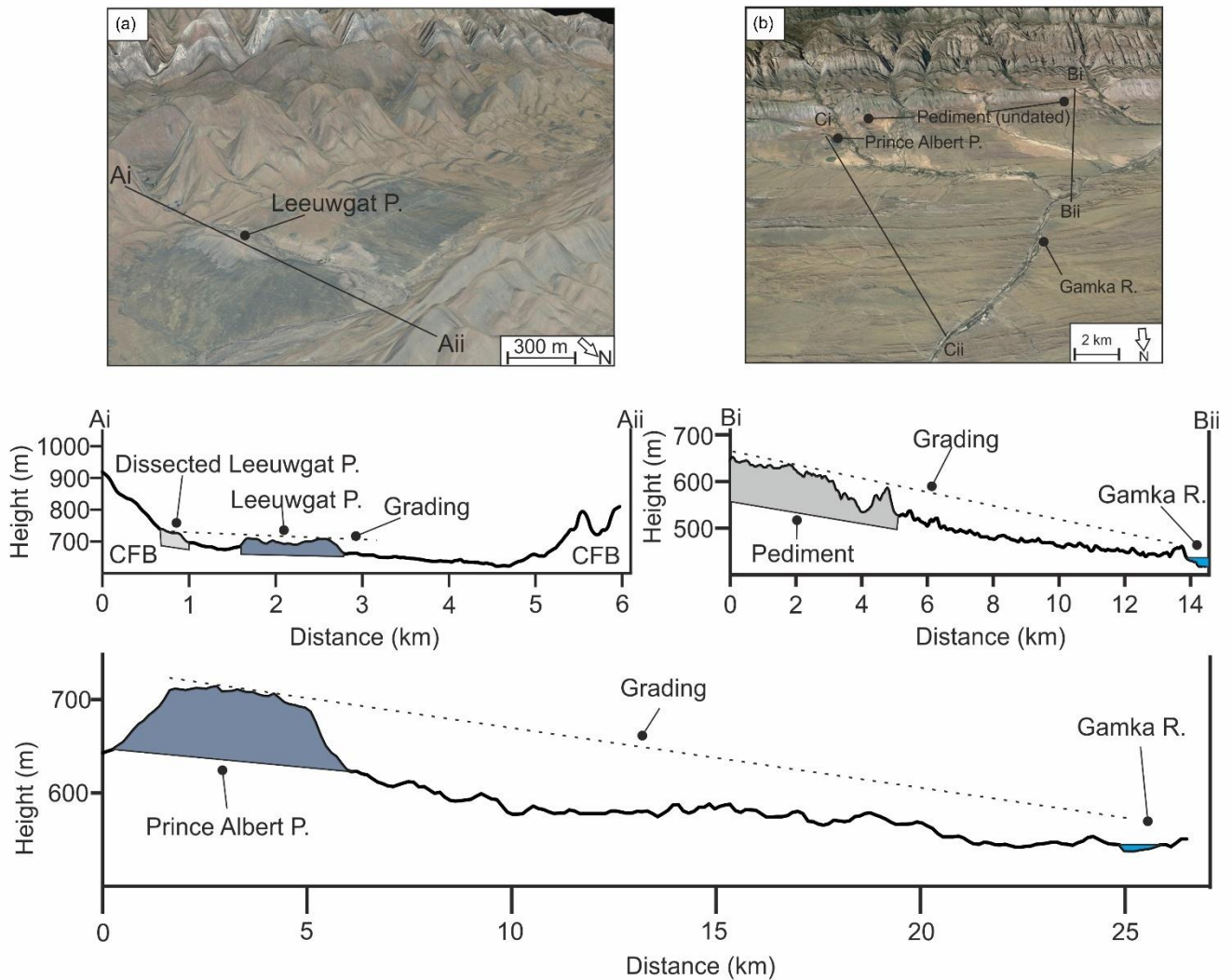


372

373 **Figure 12: Grading of the Laingsburg pediment and related cross sections, which grade not only away from the Cape**

374 **Fold Belt but towards the Buffels River. Imagery from © Google Earth 2015.**

375



376

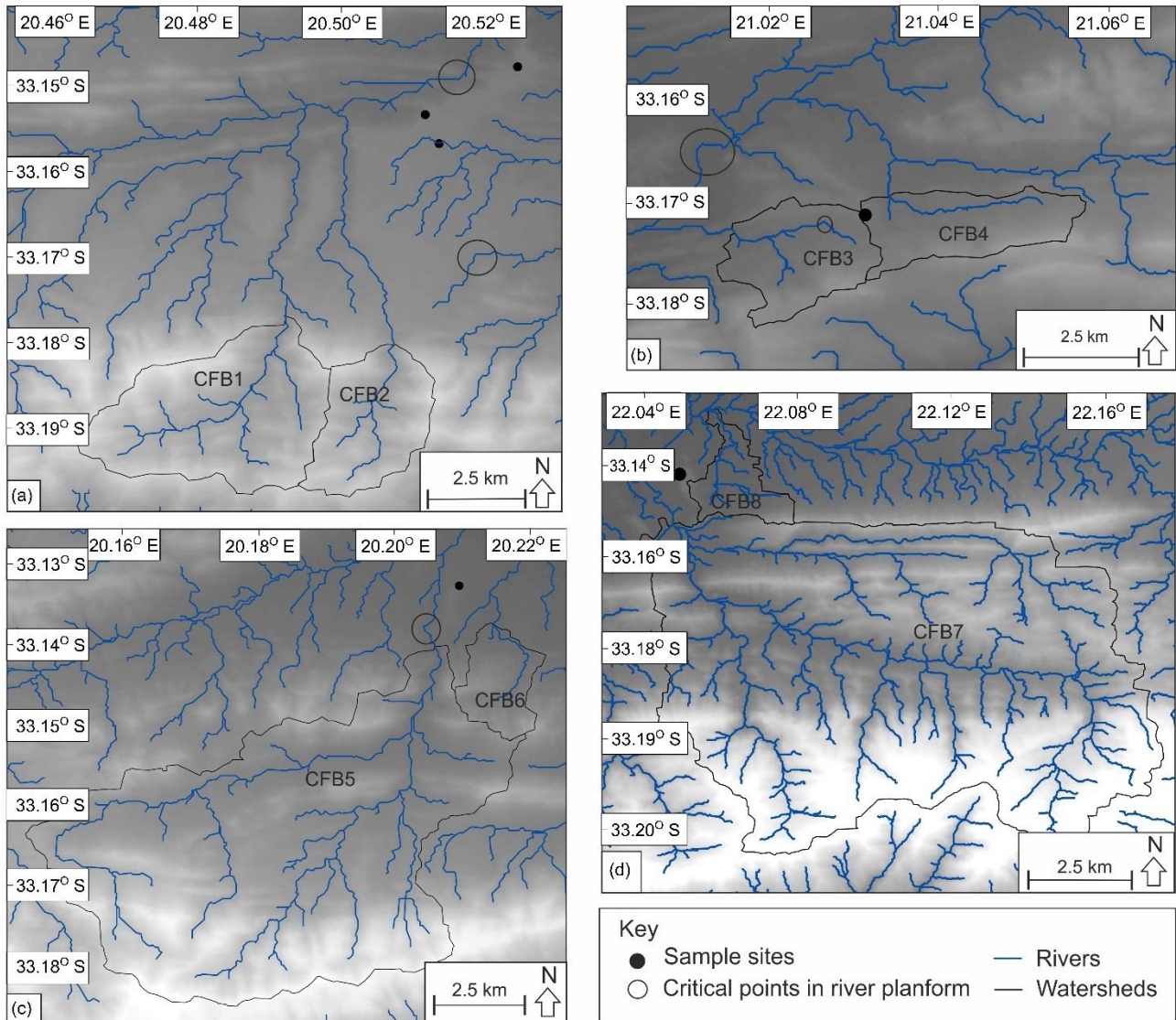
377 **Figure 13: Grading of the (a) Leeuwgat, which grades away from the Cape Fold Belt and (b) Prince Albert pediment,**
 378 **which grades towards the Gamka River. Imagery (a) and (b) from © Google Earth 2015.**

379

380 4.4. Dissecting river planform

381 The dissecting river planforms are shown in Fig. 14. Critical points are highlighted that relate to sections where the rivers (i)
 382 have been deflected by the pediment surface, or (ii) have anomalous changes in orientation. Overall, the low order rivers (<4)
 383 that have dissected the pediments are strongly influenced by the folding within the CFB (Richardson et al., 2016). This is
 384 especially seen within the rivers that have dissected the Laingsburg pediment (Fig. 14a), where the linear river planform aligns

385 with the axis of a syncline. Where the rivers breach a fold it appears that the presence of alluviated pediments deflected the
386 river planforms; this relationship can also be seen at Floriskraal and Prince Albert area alluviated pediments (Fig. 14).



387

388 **Figure 14: Planforms of the dissecting rivers and Cape Fold Belt subcatchments; (a) Laingsburg; (b) Floriskraal; (c)**
389 **Leeuwgat and; (d) Prince Albert. The circles highlight critical points related to deflection of the river planforms by the**
390 **Cape Fold Belt or the pediment.**

391 **4.5 Volume of material removed**

392 Table 4 shows the bulk erosion rates related to dissection of the alluviated pediments post-formation. Converting this to an
393 equivalent lithological thickness (dividing the volume of material removed over the area; Aguilar et al., 2011), an average of
394 141.43 m has been eroded around the large Laingsburg area pediment (Fig. 12). The Prince Albert area pediment, has an
395 average lithological thickness of 42.33 m removed. Leeuwgat has had the least amount of dissection, with 17.25 m eroded.

396 **Table 4: Minimum volume of material eroded by rivers incising the pediment surface, the equivalent rock thickness**
397 **and the time taken for incision using the average maximum denudation rate of 10.16 m My⁻¹ from Scharf et al., 2013**
398 **and Kounov et al., 2015.**

Location	Volume of material removed (km ³)	Equivalent average rock thickness (m)	Time for incision (Ma)
Laingsburg	3.240	141.43	13.92
Floriskraal	0.154	42.33	4.17
Leeuwgat	0.169	44.27	4.36
Prince Albert	0.012	17.25	1.70

399

400 Table 5 shows the volume of material eroded by rivers draining the sub-catchments in the CFB, which have dissected the
401 alluviated pediments. The sub-catchments range in size from 4.9 – 310 km², and the volume of material removed ranges from
402 0.11 - 89 km³, which is the equivalent of 21 - 286 m of lithological thickness. The alluviated pediments that are located further
403 away from the CFB range have larger dissecting catchments associated with them. For example, the Laingsburg area alluviated
404 pediment, which is backed by the CFB, has an average sub-catchment area of 14.37 km², whereas the Prince Albert area
405 alluviated pediment is located ~ 2 km from the CFB and has an average sub-catchment area of 161.83 km². These sub-
406 catchment areas are contributing to the incision of the pediments.

407

408

409

410

411

412

413 **Table 5: Minimum volume of material eroded by rivers draining the Cape Fold Belt sub-catchments, the equivalent**
 414 **rock thickness and the average time taken for incision using the average of the maximum denudation rate recorded**
 415 **from Scharf et al., 2013 and Kounov et al., 2015 of 10.16 m My⁻¹.**

Location	Catchment	Area (km ²)	Volume of material removed (km ³)	Equivalent average rock thickness (m)	Time for incision (Ma)
Laingsburg	CFB 1	19.79	2.86	144.39	14.21
	CFB 2	8.96	0.85	95.55	9.40
Floriskraal	CFB 3	6.21	0.28	45.31	4.46
	CFB 4	6.02	0.20	33.59	3.31
Leeuwgat	CFB 5	73.80	7.55	102.25	10.06
	CFB 6	4.91	0.11	21.64	2.13
Prince Albert	CFB 7	310.75	89.01	286.44	28.19
	CFB 8	12.92	0.23	17.79	1.75

416

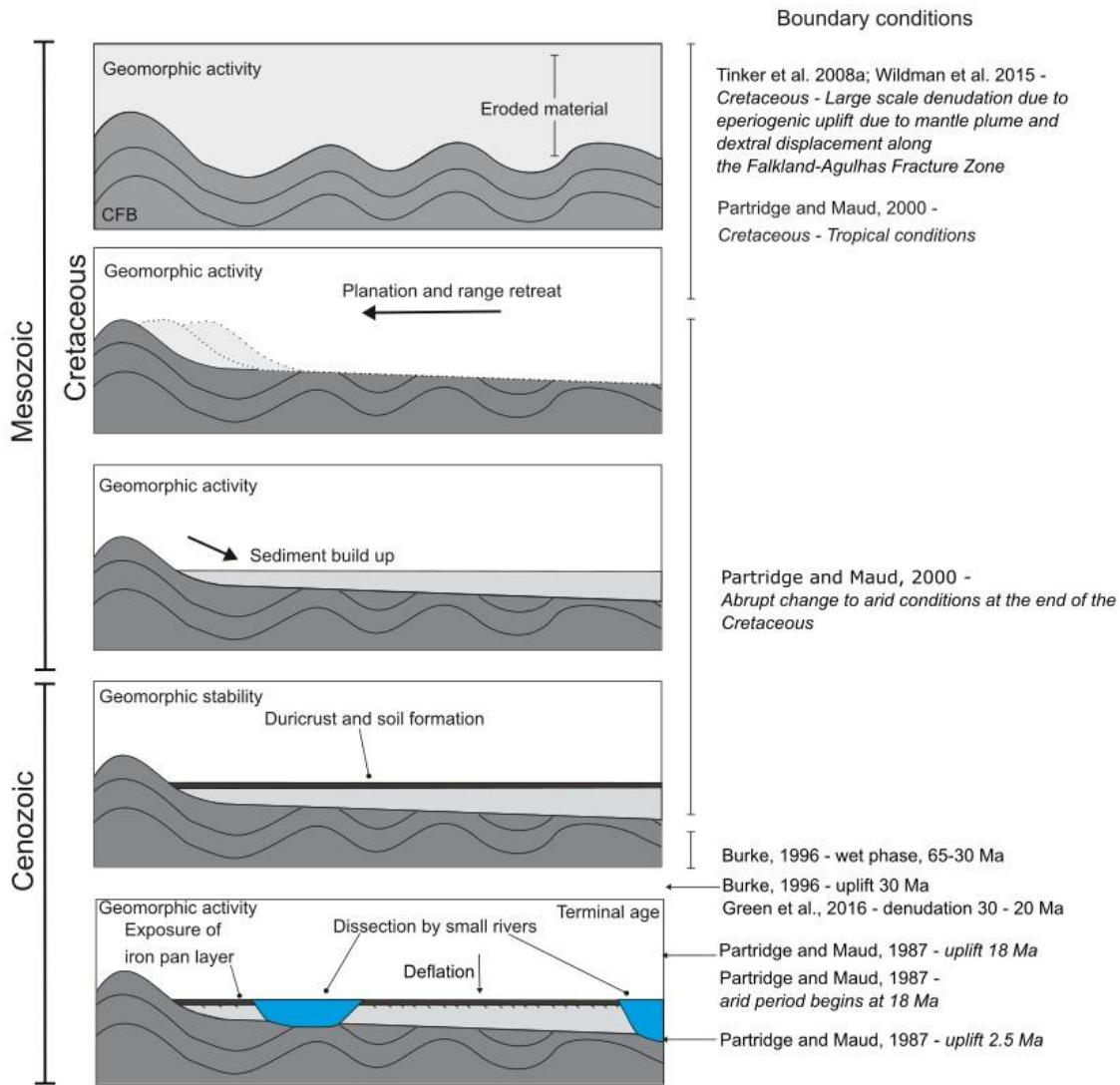
417 5. Discussion

418 5.1 Pediment formation and characteristics

419 The pediments are underlain by folded strata of the Karoo and Cape Supergroups (sandstone, siltstone and mudstone), and
 420 backed by the resistant CFB quartzites (Fig. 4b). It has been argued that pediments form on all lithology types, however the
 421 more extensive pediments can be found on less resistant material (Dohrenward and Parsons, 2009). There is no systematic
 422 variation in pediment characteristics that can be related to the underlying geology (Fig. 4b).

423 The pediments have formed by diffusive processes, dominated by slope processes in the first stages of development, causing
 424 the gradual retreat of the Cape Fold Belt and coeval formation of colluvial material and weathering mantle, including an iron
 425 pan (Fig. 15). There is no evidence of fluvial activity, such as clast imbrication, depositional or erosional bedforms, or channel-
 426 forms (Fig. 6; *cf.* e.g., Gilbert, 1877; Sharp, 1940; Lustig, 1969). The iron pan layer is now at the surface of the pediment due
 427 to the removal of overlying material as a result of surface deflation by wind erosion, as shown by the cosmogenic data from
 428 the ¹⁰Be concentration depth profile (Figs. 9, 15). The pediments grade towards, but above, large trunk rivers of the Gouritz
 429 catchment (Figs. 12, 13), indicating that large transverse systems were active before pediment planation and colluvial build-
 430 up. The trunk rivers were also active during pediment formation, however they were probably less so, as shown by the build-
 431 up and preservation of material forming the pediments. This suggests that at the time of pediment formation there was
 432 deposition of colluvial material adjacent to large-scale sediment bypass via rivers, and formation of the pediment surfaces

433 because of erosion processes. The trunk rivers, active during the formation of the pediments represent an upper limit to the
 434 extent of the pediments and the pediments should be regarded as individual landforms and not as an extensive regional 'surface'
 435 within the study area (*cf.* King, 1948, 1953, 1955; Partridge and Maud, 1987).



436

437 **Figure 15: Sequence of events forming the pediments and boundary conditions; in which the folded Karoo**
 438 **Supergroup strata was planned, hillslope processes caused the build-up of sediment, soil formation and duricrust**
 439 **formation. The pediments were then dissected and fluvial processes dominate. In recent time, deflation processes**
 440 **have dominated (Fig. 10).**

441 The distribution of the dissected pediments suggests that these are remnants of much more continuous local features (Fig. 13).
442 There has been a shift in the dominant process regime, from slope processes to fluvial processes, during the evolution of the
443 pediments as evidenced by the dissection of pediments by smaller rivers and the decoupling of the pediments from the CFB
444 sediment source area. The river planform has been primarily controlled by the orientation of tectonic folds. However, the
445 pediments could have also controlled the landscape evolution by deflecting the rivers, allowing the surfaces to be preserved.
446 It appears that the structural integrity of the pediment is not continuous across the entire pediment. Areas underlain by cohesive
447 material caused deflection of the dissecting rivers due to a higher resistance to erosion (Fig. 14). This could be a function of
448 the sedimentology (Fig. 6) of the pediment: the calibre of material; the extent of packing; or the presence and thicknesses of
449 the duricrust layer. Deflection of rivers has been shown to cause the formation of epigenetic gorges (Ouimet et al., 2008).
450 Furthermore, the pediments could have been preserved in these locations as rivers did not migrate laterally, which could be
451 due to variations in channel gradient. The pediments sit above the valley floor (current level of erosion) and are fossilised
452 landforms that represent a store of sediment that is mostly subject to slow denudation and weathering, followed by deflation
453 under current climatic conditions (Fig. 10). Hillslope processes have slowly supplied sediment to the nearby fluvial channels;
454 however due to slow runoff rates related to the arid climate, the transport is no longer effective.

455

456 **5.2 Implications of depth profile**

457 The ^{10}Be concentration depth profile (Fig. 9a) in the Laingsburg pediment deviates from a simple exponential concentration-
458 depth profile. The stronger than theoretically expected decrease in ^{10}Be concentrations in the upper 30 cm points to a complex
459 post-depositional history of the alluviated pediment. The deviation can be explained by a long phase of low denudation rate
460 (0.3 to 0.6 m/My) followed by aeolian deflation whereby finer material is preferentially removed. Deflation has been reported
461 for (semi-)arid environments during the Cenozoic (Binnie et al. 2020). The impact of deflation on ^{10}Be concentrations has been
462 described for glacial outwash terraces (Hein et al. 2009; Darvill et al. 2015) where aeolian deflation and bio- or cryoturbation
463 caused previously buried cobbles to become exposed. It has also been recorded for periglacial areas of central Europe where
464 depth profiles revealed denudation rates of 40 to 80 m My^{-1} during the Quaternary (Ruszkiczay-Rudiger et al. 2011). Binnie
465 et al. (2020) showed that deflation on marine terraces in Northern Chile is the primary cause for multimodal distributions of
466 ^{10}Be concentration depth profiles. Although the climate in southern South Africa has become more arid since the Cenozoic,
467 the impact of aeolian deflation on ^{10}Be concentrations of pediment surfaces has not yet been addressed in previous work.
468 Further work is needed to understand if this behaviour is apparent across other pediment surfaces in the area, and how common
469 this feature is across other pediment surfaces.

470 Our results also warrant for potential bias that can arise when collecting only surface samples from alluvial pediments. Boulders
471 armoring the surface of alluvial pediments can be enriched in ^{10}Be concentrations, compared to the sandy matrix, as they are
472 residual features. Their in-situ produced ^{10}Be concentrations are pertinent to reconstructing exposure ages but underestimate

473 surface process rates. In contrast, sampling sand-sized material from the surface would have yield erroneous inferred ages that
474 are too young (Fig. 9b). There is an added value in sampling pediments at min. three depths covering a full path attenuation
475 length, as additional information on erosion-exposure age scenarios can be provided.

476 **5.3 Geomorphic, tectonic, climatic and stratigraphic considerations**

477 The cosmogenic data presented in Table 3 and Fig. 9 is within the range of data presented in Fig. 3 (van der Wateren and
478 Dunai, 2001; Bierman et al., 2014; Kounov et al., 2015). There is no systematic spatial variation in surface lowering rates of
479 the pediments that can be correlated to pediment size, or geology. The Prince Albert area alluviated pediment is the most
480 isolated from the CFB, with no duricrust present (Fig. 4a), which can explain why the surface lowering rates are the highest in
481 this location (0.954 m My^{-1} compared to a maximum of 0.587 m My^{-1} for the other pediments). Further, the pediment surfaces
482 only remain fossilised as long as the duricrust remains. When the duricrust is removed, denudation rates likely increase slightly
483 as shown by the Prince Albert area alluviated pediment, but will still remain low compared to other landforms (Fig. 3, Table
484 3). Therefore, the duricrusts represent an intrinsic geomorphic threshold. By using forward modelling on the depth profile in
485 the Laingsburg pediment, we demonstrated that the ^{10}Be concentrations are at secular equilibrium, and that the pediment has
486 been exposed for more than 2 My (Fig. 11).

487

488 The volume of material removed by river incision into the pediment surfaces equates to a lithological thickness of 42 to 141
489 m (Table 4). Assuming an average maximum denudation rate of the surrounding CFB area (10.16 m My^{-1} from Scharf et al.,
490 2013 and Kounov et al., 2015), we can estimate that the dissection started as early as ~2 to 14 Ma ago. Cosmogenic and
491 thermochronological (apatite fission track and (U-Th)/He) studies have reported low denudation rates across the Cenozoic,
492 and Scharf et al. (2013) stated that the close agreement between the CRN-based denudation and AFTA/(U-Th)/He exhumation
493 rates is indicative of relative tectonic stability over the last 10^6 to 10^8 years.

494

495 As the dissection would have occurred after the formation of the alluviated pediments, they need to be older than the start of
496 the incision phase (2- 14 My). Based on the observed denudation of the sub-catchments within the CFB that back the pediments
497 and the mean maximum denudation rates from Scharf et al. 2013 and Kounov et al. 2015 (Figs. 3 and 8, Table 5), we obtain
498 indicative minimum ages of 9 - 14 My for the Laingsburg area pediment, 3 - 4 My for Floriskraal, 2 - 10 My for Leeuwgat and
499 2 - 28 My for Prince Albert. The CFB subcatchment denudation ages represent the ages of the dissecting rivers reaching the
500 CFB after dissecting the pediment surfaces. These indicative ages must be taken with caution as maximum published rates
501 have been used, and denudation rates vary over time, with a phase of increased erosion likely forming the incised channels.
502 Furthermore, as shown by the pediments causing the deflection of surrounding rivers (Fig. 14), denudation of the pediment is
503 slow (estimated between 0.3 and 0.6 m My^{-1}) as the resistance of the pediment is higher than the surrounding bedrock in some
504 locations.

505

506 Using a combination of the data above, including data on the dissection of the pediment and backing subcatchments eroded
507 into the resistant Cape Fold Belt Catchments, the Laingsburg area pediment could have an age of 23 Ma; Floriskraal 8 Ma;
508 Leeuwgat 10 Ma; and Prince Albert 17 Ma. These age estimates correspond to the start of dissection, and are based on the
509 assumption that geomorphic process rates were steady over long timescales. The geomorphic evidence corroborates the
510 outcomes of the numerical simulations of possible erosion-exposure age scenarios for the Laingsburg pediment, uncovering
511 the possibility of having very old (3 to > 15 My) exposed surfaces. If the cosmogenic *minimum* exposure ages are used, with
512 the volume eroded recorded using the DEM, erosion rates range from 28 to 503 m Ma⁻¹ which further indicates the minimum
513 exposure ages should be taken with caution as these extremely high erosion rates have not been recorded using published
514 studies (Fig. 3). Previous works have classified pediment surfaces within height brackets (e.g., King, 1953). However, in this
515 study there is no correlation between pediment elevation and their geomorphic ages.

516

517 Duricrusts are found in many of the studied alluviated pediments (Summerfield, 1983; Marker et al., 2002), and this is well-
518 developed in the Laingsburg area pediment (Fig. 5). The alluviated pediments no longer have the overlying weathering material
519 preserved, and have been lowered to the iron pan layer. The depth profile suggests that erosion has occurred after the
520 development of the weathering mantle (Fig. 9), which has exposed the iron pan (laterites). The iron pan could have formed by
521 leaching from surrounding lithologies and clasts, by lateral movement due to groundwater change (Widdowson, 2007), or by
522 deep weathering of the bedrock. Deep weathering with the formation of iron pans occurs on low relief surfaces that have been
523 stable for at least a million years (Al-Subbary et al., 1998). Since the Cenozoic, South Africa has been relatively tectonically
524 quiescent (e.g., Bierman et al., 2014). In addition, a favourable climate of high annual rainfall, high humidity and high mean
525 annual temperature is required to form laterites (Widdowson, 2007). Further, higher concentrations of carbon dioxide are also
526 associated with the formation of laterites (and iron pans). Greenhouse episodes have occurred in the late Cretaceous and late
527 Palaeocene to early Eocene, leading to world-wide extensive weathering (Bardossy, 1981; Valeton, 1983).

528 Laterite development in southern South Africa is still poorly constrained. It has been argued to be late Pliocene in age (Marker
529 and Holmes, 1999) and have continued into the late Pleistocene (Marker and Holmes, 2005), being a component of the
530 Quaternary development of the Southern Cape (Marker et al., 2002). However, the Mediterranean climate (e.g., more humid)
531 of the coastal areas does not extend inland to the study location, which is expected for laterite development (Brown et al.,
532 1994; Braucher et al 1998a, b). Given the past climate and tectonic events, the iron pans probably formed during the late
533 Cretaceous greenhouse episode, which is compounded by the constrained dissection rates of the pediment surfaces (e.g.,
534 Dauteuil et al., 2015). The formation of duricrusts and iron pans would have occurred coevally with pediment formation, and
535 would have extended post-pediment formation (Helgren and Butzer, 1977; Widdowson, 2007). The presence of iron pans
536 indicates a period of geomorphic stability that can have lasted more than 2 My with low (0.3 to 0.6 m My⁻¹) denudation rates.

537 **5.4 Sequence of events**

538 Pediment formation requires mountain range retreat, which causes the underlying lithological strata to be truncated (Fig. 15).
539 The *minimum* exposure ages calculated by cosmogenic nuclide dating using the boulder surface samples show remarkably low
540 denudation rates of the pediments during the last 3.8 Myr, which is related both to lithology (duricrust cappings, resistant
541 quartzite boulders; e.g., Scharf et al., 2013) and structure of the CFB deflecting incising rivers.

542 During the Cretaceous the Cape Fold Belt was exhumed (Fig. 15; Tinker et al. 2008a, Tankard et al. 2009). During this time,
543 the folded strata was eroded and planed by hillslope processes (e.g., Rich, 1935; Bourne and Twidale, 1998), depositing
544 colluvial material and then forming soils (Fig. 15) on the alluviated pediments. This was aided by the humid climate and
545 greenhouse conditions of the Cretaceous causing deep weathering (Bardossy, 1981; Valeton, 1983). Tectonic stability allowed
546 the formation of iron pans and duricrusts, which are now exposed at the surface of the alluviated pediments due to surface
547 deflation and the removal of overbank material, as shown by the depth profile (Fig. 15). The initial planation and colluvial
548 build-up had to have occurred pre-Miocene as shown by the dissection data (Tables 4, 5). However, we posit the surfaces could
549 have formed much earlier due to the very slow processes associated with pediment formation (e.g., Lustig, 1969; Dohrenwend
550 and Parsons, 2009). By the mid-Miocene, dissection of the pediments and backing Cape Fold Belt occurred with the
551 development of small streams and subcatchments draining the pediments, with a shift towards a more fluvial dominated regime.
552 This latter stage of landscape development has decoupled the pediments from the CFB sediment source, and essentially
553 fossilised the landform (Table 3), with very low denudation (0.3 to 0.6 m My^{-1}) followed by a more recent phase of aeolian
554 deflation.

555 **5.5 Implications for landscape development**

556 The evolution of the pediment surfaces studied in South Africa indicates that the relative importance of hillslope and fluvial
557 processes (including valley development) varies over time. Therefore, the model proposed here does not fit into the previously
558 published model types (Fig. 1) that argued that pediment evolution is dominated by a single process (e.g., ‘Model 1’ Figure 1;
559 Gilbert, 1877; Paige, 1912; Howard 1942 and ‘Model 2’ Fig. 1; Lawson, 1915; Rich; 1935; Kesel, 1977; Bourne and Twidale,
560 1998; Dauteuil et al., 2015), that the dominant process varies due to lithology (e.g., ‘Model 3’ Figure 1: Lustig, 1969; Parsons
561 and Abrahams, 1984) or is assisted by valley/basin development (e.g., ‘Model 4’ Fig. 1; Lustig, 1969; Parsons and Abrahams,
562 1984). The change from hillslope to fluvial processes is likely a response to tectonic or climatic perturbations (Fig. 15). The
563 initial formation of the pediments was most likely aided by large-scale erosion during the Cretaceous (e.g., Tinker et al.,
564 2008a,b; Wildman et al., 2015, 2016; Richardson et al., 2017) and tropical climate conditions (Partridge and Maud, 2000).

565 The indicative geomorphic ages reported here, related to the second phase of development and the dissection of the pediments
566 by small tributaries, roughly correlate to the proposed uplift in the Cenozoic (Green et al., 2016) of 30 Ma (Burke, 1996), 18
567 Ma (Partridge and Maud, 1987) and 2.5 Ma (Partridge and Maud, 1987), and could indicate that the pediments were dissected

568 due to different pulses of uplift. Nonetheless, this time period also corresponds to variation in climate, including periods of
569 humidity reported to have ended at 30 Ma (Burke, 1996) or 18 Ma (Burke, 1996). It is not possible to distinguish the main
570 driver of dissection, and tectonic signatures are not identified within the Gouritz catchment morphometry (Richardson et al.,
571 2016).

572 The grading of the pediments implies that the main trunk rivers were active before the development of the pediments, at least
573 by the Miocene and probably within the Cretaceous when large scale exhumation occurred within South Africa (e.g., Tinker
574 et al. 2008a, Richardson et al., 2017). The individual grading of the pediment surfaces indicates the pediments are relatively
575 local features that react to surrounding tectonic, geological, and geomorphological settings, and are not singular surfaces (King,
576 1953). The ^{10}Be -derived denudation rates of the pediments are some of the lowest in the world (Portenga and Bierman, 2011),
577 and congruent with low geomorphic activity documented by other researchers (Fig. 3, and references therein). There has been
578 a drastic reduction in denudation rates since the Cretaceous as shown by apatite fission track and cosmogenic nuclide studies
579 (Fig. 3 and references therein). However, surface lowering is not consistent across landforms within southern South Africa.
580 Rivers are dissecting at a faster rate (Scharf et al., 2013; Kounov et al., 2015) than the pediment surfaces (this study, van der
581 Wateren and Dunai, 2001; Bierman et al., 2014; Kounov et al., 2015), which indicates that relief is developing at a slow rate,
582 as also reported by Bierman et al. (2014) from the Eastern Cape. The offshore depositional record (Tinker et al. 2008a) mirrors
583 the reduction in denudation rates with peaks in the Cenozoic most likely related to the rejuvenation of the landscape, which
584 dissected the pediments in this study (e.g., Hirsch et al., 2010; Dalton et al., 2015; Sonibare et al., 2015). These increases in
585 offshore sediment flux are minor in comparison to rates in the Cretaceous.

586 **6. Conclusion**

587 Large-scale erosional surfaces characterise the ancient landscape of southern South Africa. Denudation rates of the Prince
588 Albert and Laingsburg pediments in the Western Cape are between 0.3 and 1.0 m My^{-1} , and the pediments have been exposed
589 before the Early Pleistocene. As most of the pediment surfaces have ^{10}Be concentrations that approach secular equilibrium,
590 the ^{10}Be -derived exposure ages provide minimum exposure age estimates. Our study corroborates how CRN depth profiling
591 in alluvial pediments can provide additional information on long-term landscape dynamics, and demonstrates how forward
592 modelling can unveil the erosion-exposure age scenarios that most likely explain the observed ^{10}Be depth concentrations. The
593 existence of a long period of low denudation followed by a recent phase of aeolian deflation merits further study to verify if
594 this is a widespread and characteristic feature of alluviated pediment surfaces in (semi-)arid climatic conditions.

595 The pediments studied must be at least Miocene in age, and probably much older (i.e. Cretaceous) based on the volumes of
596 post-pediment dissection, published erosion rates, the presence of duricrusts and the current understanding of tectonic and
597 climatic variation in the region. The duricrusts represent an internal geomorphic threshold which limits the rate of denudation.
598 The dissection of the pediments has been largely controlled by the structure of the Cape Fold Belt, with the initial geomorphic

599 pulse of incision most likely related to tectonic uplift or climate change. The pediments grade to individual base levels (trunk
600 rivers), and although locally extensive, they are not a regional feature representing one single surface. The presence of the
601 pediments deflected dissecting rivers in some locations and controlled landscape evolution of the surrounding rivers.

602 The pediments in southern South Africa are lowering at very low rates and are now decoupled from the surrounding rivers.
603 Therefore, they are a fossilised landform that represents a relatively stable store of sediment in which surface lowering occurs
604 by aeolian erosion causing deflation. The persistence of the pediments is due to the resistant duricrust capping and quartzitic
605 boulders, and the structural control of the Cape Fold Belt and pediments, deflecting dissecting rivers. We contend that a multi-
606 proxy approach that combines cosmogenic nuclides with surrounding geomorphologic and stratigraphic conditions provides a
607 more comprehensive picture of long-term landscape dynamics.

608

609 **Data availability**

610 Cosmogenic data used in this study is provided as a supplement.

611 **Author Contributions**

612 Janet C. Richardson, David Hodgson and Andreas Lang collected the data. Processing and analysis of the data was completed
613 by Janet C. Richardson and Veerle Vanacker. Forward modelling work was completed by Veerle Vanacker. Marcus Christl
614 measured the $^{10}\text{Be}/^9\text{Be}$ using an accelerator mass spectrometer on the 500 kV Tandy facility at ETH Zürich. Veerle Vanacker
615 provided further support processing the data with regards to the depth profile, creating Figure 9 and writing the methodology
616 for cosmogenic nuclides. Janet C. Richardson led the writing and drafting of figures, with contributions on the text and figures
617 by Veerle Vanacker, David Hodgson and Andreas Lang.

618 **Acknowledgements**

619 The British Geomorphology Society (BSG) and British Sedimentology Research Group (BSRG) are thanked for providing
620 postgraduate grants to J. Richardson for completing this research. Jérôme Schoonejans and Marco Bravin are thanked for their
621 help during laboratory work undertaken in Université catholique de Louvain, Belgium. David Lee is thanked for his help in
622 improving Fig. 1. The landowners in South Africa are thanked for their permission to enter their land and take samples. The
623 Council of Geoscience are thanked for providing Geology GIS tiles, under the Academic/Research license. Alexandre Kounov
624 and an anonymous reviewer are thanked for their reviews of a previous version of this paper.

625

626 **Competing interests**

627 Andreas Lang is a member of the editorial board for Earth Surface Dynamics.

628 **References**

629 Abdelkareem, M., Ghoneim, E., El-Baz, F., and Askalany, M.: New insight on paleoriver development in the Nile basin of the
630 eastern Sahara. *J. of Afr. Ear. Sci.*, 62, 35-40, doi: 10.1016/j.jafrearsci.2011.09.001, 2012.

631 Aguilar, G., Riquelme, R., Martinod, J., Darrozes, J. and Maire, E.: Variability in erosion rates related to the state of landscape
632 transience in the semi-arid Chilean Andes. *ESPL*, 36, 1736-1748, doi: 10.1002/esp.2194, 2011.

633 Al-Subbary, A.K., Nichols, G.J., Bosence, D.W.J. and Al-Kadasi, M.: Pre-rift doming, peneplanation or subsidence in the
634 southern Red Sea? Evidence from the Medj-Zir Formation (Tawilah Group) of western Yemen. In: Purser BH, Bosence D.
635 (eds.) *Sedimentation and Tectonics in Rift Basins Red Sea:-Gulf of Aden*. Springer Netherlands. pp. 119-134, 1998

636 Balco, G., Stone, J.O., Lifton, N.A. and Dunai, T.J.: A complete and easily accessible means of calculating surface exposure
637 ages or erosion rates from 10 Be and 26 Al measurements. *Q. Geochron.*, 3: 174-195, doi: 10.1016/j.quageo.2007.12.001,
638 2008.

639 Bardossy, G.: Paleoenvironments of laterites and lateritic bauxites – effect of global tectonism on bauxite formation. In:
640 *International Seminar on Lateritisation Processes (Trivandrum, India)*. Rotterdam: Balkema, pp. 284–297, 1981

641 Bellin N, Vanacker V, Kubik PW. Denudation rates and tectonic geomorphology of the Spanish Betic Cordillera. *EPSL*, 390:
642 19-30, doi: 10.1016/j.epsl.2013.12.045, 2014.

643 Bessin, P., Guillocheau, F., Robin, C., Schrötter, J.M., Bauer, H.: Planation surfaces of the Armorican Massif (western France):
644 Denudation chronology of a Mesozoic land surface twice exhumed in response to relative crustal movements between Iberia
645 and Eurasia. *Geomorph.*, 233: 75-91, doi: 10.1016/j.geomorph.2014.09.026, 2015.

646 Bierman, P.R. and Caffee, M.: Slow rates of rock surface erosion and sediment production across the Namib Desert and
647 escarpment, southern Africa. *Am. J. Sci.*, 301, 326-358, 2001.

648 Bierman, P.R., Coppersmith, R., Hanson, K., Neveling, J., Portenga, E.W. and Rood, D.H.: A cosmogenic view of erosion,
649 relief generation, and the age of faulting in southern Africa. *GSA Today*, 24: 4-11, doi: 10.1130/GSATG206A.1, 2014.

650 Binnie, A., Binnie, S.A., Parteli, E.J.R. and Dunai, T.J.: The implications of sampling approach and geomorphological
651 processes for cosmogenic 10Be exposure dating of marine terraces. *Nucl. Instrum. and Methods Phys. Res. Sec. B*, 467, 130-
652 139, doi: 10.1016/j.nimb.2019.12.017 , 2020.

653 Bishop, P.: Long-term landscape evolution: linking tectonics and surface processes. *ESPL*, 32: 329-365, doi:
654 10.1002/esp.1493, 2007.

655 Bloom, A.L.: Teaching about relict, no-analog landscapes. *Geomorph.*, 47: 303-311, doi: 10.1016/S0169-555X(02)00094-6 ,
656 2002.

657 Bourne, J.A. and Twidale, C.R.: Pediments and alluvial fans: genesis and relationships in the western piedmont of the Flinders
658 Ranges, South Australia. *Aust. J. Earth Sci.*, 45: 123–135, doi: 10.1080/08120099808728373, 1998.

659 Braucher, R., Bourles, D.L., Colin, F., Brown, E.T. and Boulange, B.: Brazilian laterite dynamics using in situ-produced 10
660 Be. *EPSL*, 163: 197-205, doi: 10.1016/S0012-821X(98)00187-3, 1998.

661 Braucher R., Colin, F., Brown, E.T., Bourles, D.L., Bamba, O., Raisbeck, G.M., You, F. and Koud, J.M.: African laterite
662 dynamics using in situ-produced 10 Be. *Geochem. Cosmo. Acta*, 62, 1501-1507, doi: 10.1016/S0016-7037(98)00085-4, 1998.

663 Braucher, R., Brown, E.T., Bourlès, D.L. and Colin, F.: In situ produced 10 Be measurements at great depths: implications for
664 production rates by fast muons. *EPSL*, 211, 251-258, doi: 10.1016/S0012-821X(03)00205-X, 2003.

665 Braucher, R., Merchel, S., Borgomano, J. and Bourlès, D.L.: Production of cosmogenic radionuclides at great depth: A
666 multielement approach, *EPSL*, 309, 1–9, doi: 10.1016/j.epsl.2011.06.036 , 2011.

667 Braun, J., Guillocheau, F., Robin, C., Baby, G. and Jelsma, H.: Rapid erosion of the Southern African Plateau as it climbs over
668 a mantle superswell. *J. Geophys. Res.: Solid Earth*: 119, 6093-6112, doi: 10.1002/2014JB010998, 2014.

669 Brocklehurst, S.H. and Whipple, K.X.: Glacial erosion and relief production in the Eastern Sierra Nevada, California.
670 *Geomorph.*, 42, 1–24, doi: 10.1016/S0169-555X(01)00069-1, 2002.

671 Brook, E.J., Brown, E.T., Kurz, M.D., Ackert, R.P., Raisbeck, G.M. and Yiou, F.: Constraints on age, erosion, and uplift of
672 Neogene glacial deposits in the Transantarctic Mountains determined from in situ cosmogenic 10Be and 26Al. *Geol.*, 23, 1063-
673 1066, doi: 10.1130/0091-7613(1995)023<1063:COAEAU>2.3.CO;2, 1995.

674 Brown, E.T., Bourlès, D.L., Colin, F., Sanfo, Z., Raisbeck, G.M., and Yiou, F.: The development of iron crust lateritic systems
675 in Burkina Faso, West Africa examined with in-situ-produced cosmogenic nuclides. *EPSL*, 124, 19-33, doi: 10.1016/0012-
676 821X(94)00087-5, 1994.

677 Brown, R.W., Rust, D.J., Summerfield, M.A., Gleadow, A.J. and De Wit, M.C.: An Early Cretaceous phase of accelerated
678 erosion on the south-western margin of Africa: Evidence from apatite fission track analysis and the offshore sedimentary
679 record. *Int. J. Rad. Appl. Instr. A. Part D. Nucl. Tracks and Radiat. Meas.*, 17, 339-350, doi: 10.1016/1359-0189(90)90056-
680 4, 1990.

681 Brown, R.W., Summerfield, M.A. and Gleadow, A.J.W.: Denudation history along a transect across the Drakensberg
682 Escarpment of southern Africa derived from apatite fission track thermochronology. *J. Geophys. Res.*, 107, 1-18, doi:
683 10.1029/2001JB000744, 2002.

684 Bryan, K.: Erosion and sedimentation in the Papago country, Arizona. *U.S Geol. Surv. Bull.*, 730, 19–90, 1923.

685 Burbank, D.W., Leland, J., Fielding, E., Anderson, R.S., Brozovic, N., Reid, M.R. and Duncan, C.: Bedrock incision, rock
686 uplift and threshold hillslopes in the northwestern Himalayas. *Nature*, 379, 505-510, 1996.

687 Burke, K. The African plate. *S. Afri. J. Geol.*, 99, 341-409, 1996.

688 Carignano, C., Cioccale, M., and Rabassa, J.: Landscape antiquity of the Central Eastern Sierras Pampeanas (Argentina):
689 Geomorphological evolution since Gondwanic times. *Z. Geomorph. Supplement Band* 118, 245–268, 1999.

690 Chadwick, O.A., Roering, J.J., Heimsath, A.M., Levick, S.R., Asner, G.P. and Khomo, L.: Shaping post-orogenic landscapes
691 by climate and chemical weathering. *Geol.*, 41, 1171-1174, doi: 10.1130/G34721.1, 2013.

692 Chappell, J., Zheng, H. and Fifield, K.: Yangtse River sediments and erosion rates from source to sink traced with cosmogenic
693 ¹⁰Be: Sediments from major rivers. *Palaeo.*, 241, 79-94, doi: 10.1016/j.palaeo.2006.06.010, 2006.

694 Chmeleff, J., von Blanckenburg, F., Kossert, K. and Jakob, D.: Determination of the ¹⁰Be half-life by multicollector ICP-MS
695 and liquid scintillation counting. *Nucl. Instrum. and Methods in Phys. Res. B*, 263, 192–199, doi: 10.1016/j.nimb.2009.09.012,
696 2010.

697 Chorley, R.J., Schumm, S.A. and Sugden, D.E.: *Geomorphology*, London. Methuen and Co. 648 pp, 1984.

698 Christl, M., Vockenhuber, C., Kubik, P.W., Wacker, L., Lachner, J., Alfimov, V. and Synal, H.-A.: The ETH Zurich AMS
699 facilities: Performance parameters and reference materials. *Nucl. Instrum. and Methods in Phys. Res. B*, 294, 29-38, doi:
700 10.1016/j.nimb.2012.03.004, 2-13, 2013.

701 Cockburn, H.A.P., Brown, R.W., Summerfield, M.A. and Seidl, M.A.: Quantifying passive margin denudation and landscape
702 development using a combined fission-track thermochronology and cosmogenic isotope analysis approach. *EPSL*, 179, 429-
703 435, doi: 10.1016/S0012-821X(00)00144-8, 2000.

704 Codilean, A.T., Bishop, P., Stuart, F.M., Hoey, T.B., Fabel, D. and Freeman, S.P.: Single-grain cosmogenic ²¹Ne
705 concentrations in fluvial sediments reveal spatially variable erosion rates. *Geol.*, 36, 159-162, doi: 10.1130/G24360A.1, 2008.

706 Dalton, T.J.S., Paton, D.A., Needham, T. and Hodgson, N.: Temporal and spatial evolution of deepwater fold thrust belts:
707 Implications for quantifying strain imbalance. *Interpret.*, 3, SAA59-SAA70, doi: 10.1190/INT-2015-0034.1, 2015.

708 Darvill, C.M., Bentley, M.J., Stokes, C.R., Hein, A.S. and Rodés, Á.: Extensive MIS 3 glaciation in southernmost Patagonia
709 revealed by cosmogenic nuclide dating of outwash sediments. *EPSL*, 429, 157-169, doi: 10.1016/j.epsl.2015.07.030, 2015.

710 Dauteuil, O., Bessin, P. and Guillocheau, F.: Topographic growth around the Orange River valley, southern Africa: A Cenozoic
711 record of crustal deformation and climatic change. *Geomorph.*, 233, 5-19, doi: 10.1016/j.geomorph.2014.11.017, 2015.

712 Davis, W.M. Observations in South Africa. *Geol. Soc. Am. Bull.*, 17, 377-450, 1906.

713 Dean, W.R.J., Hoffinan, M.T., Meadows, M.E. and Milton, S.J.: Desertification in the semi-arid Karoo, South Africa: review
714 and reassessment. *J. Arid Env.*, 30, 247-264, doi: 10.1016/S0140-1963(05)80001-1, 1995.

715 Decker, J.E., Niedermann, S. and de Wit, M.J.: Soil erosion rates in South Africa compared with cosmogenic ³He-based rates
716 of soil production. *S. Afri. J. Geol.*, 114, 475-488, doi: 10.2113/gssajg.114.3-4.475, 2011.

717 Decker, J.E., Niedermann S. and de Wit, M.J.: Climatically influenced denudation rates of the southern African plateau: Clues
718 to solving a geomorphic paradox. *Geomorph.*, 190, 48-60, doi: 10.1016/j.geomorph.2013.02.007, 2013.

719 Doucouré, C.M. and de Wit, M.J.: Old inherited origin for the present near-bimodal topography of Africa. *J. Afr. Earth Sci.*,
720 36, 371-388, doi: doi.org/10.1016/S0899-5362(03)00019-8, 2003

721 Demoulin, A., Zárata, M. and Rabassa, J.: Long-term landscape development: a perspective from the southern Buenos Aires
722 ranges of east central Argentina. *J. S Am. Earth Sci.*, 19, 193–204, doi: 10.1016/j.jsames.2004.12.001, 2005.

723 De Smith, M.J., Goodchild, M.F. and Longley, P.: Geospatial analysis: a comprehensive guide to principles, techniques and
724 software tools. Troubador Publishing Ltd. pp. 389, 2007.

725 de Wit M.: The Kalahari Epeirogeny and climate change: differentiating cause and effect from core to space. *S. Afri. J. Geol.*,
726 110, 367-392, doi: 10.2113/gssajg.110.2-3.367, 2007.

727 Dirks, P.H., Kibii, J.M., Kuhn, B.F., Steininger, C., Churchill, S.E., Kramers, J.D., Pickering, R., Farber, D.L., Mériaux, A.S.,
728 Herries, A.I. and King G.C. Geological setting and age of Australopithecus sediba from southern Africa. *Sci*, 328, 205-208,
729 doi: 10.1126/science.1184950, 2010.

730 Dixey, F.: African landscape. *Geograph. Rev.*, 34, 457-465, doi: 10.2307/209976, 1944.

731 Dohrenwend, J.C. and Parsons, A.J.: Pediments in arid environments. In: Abrahams, A.D., Parsons, A.J. (Eds.)
732 *Geomorphology of desert environments*. Springer Netherlands. pp. 377-411, 2009.

733 Doucouré CM, de Wit MJ. 2003. Old inherited origin for the present near bimodal topography of Africa. *J. Afri. Earth Sci.*,
734 36, 371–388, doi: 10.1016/S0899-5362(03)00019-8, 2003.

735 Dunai, T.J.: Scaling factors for production rates of in situ produced cosmogenic nuclides: a critical reevaluation, *EPSL*, 176,
736 157-169, doi: 10.1016/S0012-821X(99)00310-6, 2000.

737 Dunai TJ. 2010. *Cosmogenic Nuclides: Principles, Concepts and Applications in the Earth Surface Sciences*, Cambridge
738 University Press, Cambridge, UK, 2010.

739 Dunai, T.J., López, G.A.G. and Juez-Larré, J.: Oligocene–Miocene age of aridity in the Atacama Desert revealed by exposure
740 dating of erosion-sensitive landforms. *Geol.*, 33, 321-324, doi: 10.1130/G21184.1, 2005.

741 Du Toit, A.: *Our Wandering Continents*. Oliver and Boyd, U.K, 366 pp, 1937.

742 Du Toit, A.: *The Geology of South Africa*, 3rd edn. Oliver and Boyd, U.K. 539 pp, 1954.

743 Ebinger, C.J. and Sleep, N.H.: Cenozoic magmatism throughout east Africa resulting from impact of a single plume. *Nature*,
744 395, 788-791, 1998.

745 Erlanger, E.D., Granger, D.E. and Gibbon, R.J.: Rock uplift rates in South Africa from isochron burial dating of fluvial and
746 marine terraces. *Geol.*, 40, 1019-1022, doi: 10.1130/G33172.1, 2012.

747 Fleming, A., Summerfield, M.A., Stone, J.O., Fifield, L.K. and Cresswell, R.G.: Denudation rates for the southern Drakensberg
748 escarpment, SE Africa, derived from in-situ-produced cosmogenic ³⁶Cl: initial results. *J. Geol. Soc.*, 156, 209-212, doi:
749 10.1144/gsjgs.156.2.0209, 1999.

750 Flowers, R.M. and Schoene, B.: (U-Th)/He thermochronometry constraints on unroofing of the eastern Kaapvaal craton and
751 significance for uplift of the southern African Plateau. *Geol.*, 38, 827-830, doi: doi.org/10.1130/G30980.1, 2010.

752 Frimmel, H.E., Fölling, P.G. and Diamond, R.: Metamorphism of the Permo-Triassic Cape Fold Belt and its basement, South
753 Africa. *Min. and Pet.*, 73, 325-346, 2001.

754 Gallagher, K. and Brown, R.: The Mesozoic denudation history of the Atlantic margins of southern Africa and southeast Brazil
755 and the relationship to offshore sedimentation. *Geol. Soc., London, Sp. Pub.*, 153, 41-53, doi: 10.1144/GSL.SP.1999.153.01.0,
756 1999.

757 Ghosh, P., Sinha, S. and Misra, A.: Morphometric properties of the trans-Himalayan river catchments: Clues towards a relative
758 chronology of orogen-wide drainage integration. *Geomorph.*, 233, 127-141, doi: 10.1016/j.geomorph.2014.10.035, 2014.

759 Gilbert, G.K.: Report on the geology of the Henry Mountains. US Geographical and Geological Survey of the Rocky Mountain
760 Region. Washington, DC: U.S. Department of the Interior, 1877.

761 Gorelov, S.K., Drenev, N.V., Mescheryakov Y.A., Tikanov, N.A. and Fridland, V.M.: Planation surfaces of the USSR.
762 *Geomorph.*, 1, 18–29, 1970.

763 Granger, D.E., Kirchner, J.W. and Finkel, R.C.: Quaternary downcutting rate of the New River, Virginia, measured from
764 differential decay of cosmogenic ²⁶Al and ¹⁰Be in cave-deposited alluvium. *Geol.*, 25, 107-110, doi: 10.1130/0091-
765 7613(1997)025<0107:QDROTN>2.3.CO;2, 1997.

766 Green, P.F., Duddy, I.R., Japsen P., Bonow, J.M. and Malan, J.A.: Post-breakup burial and exhumation of the southern margin
767 of Africa. *Basin Res.*, 29, 96 – 127, doi: 10.1111/bre.12167, 2016.

768 Guillocheau, F., Chelalou, R., Linol, B., Dauteuil, O., Robin, C., Mvondo, F., Callec, Y. and Colin, J.P.: Cenozoic landscape
769 evolution in and around the Congo Basin: constraints from sediments and planation surfaces. In: de Wit, M.J., Guillocheau, F.
770 and de Wit, M.C.J. (eds) *Geology and Resource Potential of the Congo Basin. Regional Geology Reviews*, Springer, 271-313,
771 2015.

772 Guillocheau, F., Simon, B., Baby, G., Bessin, P., Robin, C. and Dauteuil, O.: Planation surfaces as a record of mantle dynamics:
773 the case example of Africa. *Gondwana Res.*, 53, 82-98, doi: 10.1016/j.gr.2017.05.015, 2018.

774 Gunnell, Y., Braucher, R., Bourles, D. and André, G.: Quantitative and qualitative insights into bedrock landform erosion on
775 the South Indian craton using cosmogenic nuclides and apatite fission tracks. *Geol. Soc. Am. Bull.*, 119, 576-585, doi:
776 10.1130/B25945.1, 2007.

777 Hagedorn, J.: Silcretes in the Western Little Karoo and their relation to geomorphology and palaeoecology: *Palaeoecol. of*
778 *Afr.*, 19, 371–375, 1988.

779 Hansma, J., Tohver, E., Schrank, C., Jourdan, F. and Adams, D., 2016. The timing of the Cape Orogeny: New ⁴⁰Ar/³⁹Ar age
780 constraints on deformation and cooling of the Cape Fold Belt, South Africa. *Gondwana Res.*, 32, 122-137,
781 doi.org/10.1016/j.gr.2015.02.005, 2016.

782 Helgren, D.M. and Butzer, K.W.: Paleosols of the southern Cape Coast, South Africa: implications for laterite definition,
783 genesis, and age. *Geograph. Rev.*, 67, 430-445, doi: 10.2307/213626, 1977.

784 Hein, A.S., Hulton, N.R., Dunai, T.J., Schnabel, C., Kaplan, M.R., Naylor, M. and Xu, S.: Middle Pleistocene glaciation in
785 Patagonia dated by cosmogenic-nuclide measurements on outwash gravels. *EPSL*, 286, 184-197, doi:
786 10.1016/j.epsl.2009.06.026, 2009.

787 Hirsch, K.K., Scheck-Wenderoth, M., van Wees, J.D., Kuhlmann, G. and Paton, D.A.: Tectonic subsidence history and thermal
788 evolution of the Orange Basin. *Mar. Petrol. Geol.*, 27, 565-584, doi: 10.1016/j.marpetgeo.2009.06.009, 2010.

789 Howard, A.D. 1942. Pediment passes and the pediment problem. US Coast and Geodetic Survey, 1942.

790 Jackson J., Ritz, J.F., Siame, L., Raisbeck, G., Yiou, F., Norris, R., Youngson, J. and Bennett, E.: Fault growth and landscape
791 development rates in Otago, New Zealand, using in situ cosmogenic ^{10}Be . *EPSL*, 195, 185-193, doi: 10.1016/S0012-
792 821X(01)00583-0, 2002.

793 Johnson, M.R., Van Vuuren, C.J., Hegenberger, W.F., Key, R. and Show, U.: Stratigraphy of the Karoo Supergroup in southern
794 Africa: an overview. *J. African Earth Sci.*, 23, [doi.org/10.1016/S0899-5362\(96\)00048-6](https://doi.org/10.1016/S0899-5362(96)00048-6), 1995.

795 Jerolmack, D.J., Paola, C.: Shredding of environmental signals by sediment transport. *Geophys. Res. Lett.*, 37, L19401., doi:
796 10.1029/2010GL044638, 2010.

797 Kesel, R.H.: Some aspects of the geomorphology of inselbergs in central Arizona, USA. *Z. Geomorph.*, 21, 119–46, 1977.

798 Keen-Zebert, A., Tooth, S. and Stuart, F.M.: Cosmogenic ^3He measurements provide insight into lithologic controls on
799 bedrock channel incision: examples from the South African interior. *J. Geol.*, 124, 423-434, doi: 10.1086/685506, 2016.

800 King, L.C.: On the ages of African land-surfaces. *Quart. J. Geol. Soc.*, 104: 439-45, doi: 10.1144/GSL.JGS.1948.104.01-04.20,
801 1948.

802 King, L.C.: The pediment landform: some current problems. *Geol. Mag.*, 86, 245-250, doi: 10.1017/S0016756800074665,
803 1949.

804 King, L.C.: The geology of the Makapan and other caves. *Trans. Royal Soc. S. Afr.*, 33: 121-151, doi:
805 10.1080/00359195109519881, 1951.

806 King, L.C.: Canons of landscape evolution. *Geol. Soc. Am. Bull.*, 64, 721-752, doi: 10.1130/0016-
807 7606(1953)64[721:COLE]2.0.CO;2, 1953.

808 King, L.C.: Pediplanation and isostasy: an example from South Africa. *Quart. J. Geol. Soc.*, 111, 353-359, doi:
809 10.1144/GSL.JGS.1955.111.01-04.18, 1955.

810 King, L.C. 1956a. A geomorphological comparison between Eastern Brazil and Africa (Central and Southern). *Quart. J. Geol.*
811 *Soc.*, 112, 445–474, doi: 10.1144/GSL.JGS.1956.112.01-04.2, 1956a.

812 King, L.C. 1956b. A geomorfologia do Brasil oriental. *Rev. Bras. Geog.* 18,186–263, 1956b.

813 King, L.C. South African scenery. A textbook of geomorphology. 308 pp, 1963.

814 Kounov, A., Niedermann, S., de Wit, M.J., Viola, G., Andreoli, M. and Erzinger, J.: Present denudation rates at selected
815 sections of the South African escarpment and the elevated continental interior based on cosmogenic ^3He and ^{21}Ne . *S. Afri. J.*
816 *Geol.* 110, 235-248, doi: 10.2113/gssajg.110.2-3.235, 2007.

817 Kounov, A., Viola, G., De Wit, M. and Andreoli, M.A.G.: Denudation along the Atlantic passive margin: new insights from
818 apatite fission-track analysis on the western coast of South Africa. *Geol. Soc. London, Sp. Pub.*: 324, 287-306, doi:
819 10.1144/SP324.19, 2009.

820 Kounov, A., Niedermann, S., de Wit, M.J., Codilean, A.T., Viola, G., Andreoli, M. and Christl, M.: Cosmogenic ^{21}Ne and
821 ^{10}Be reveal a more than 2 Ma Alluvial Fan Flanking the Cape Mountains, South Africa. *S. Afr. J. Geol.*, 118, 129-144, doi:
822 10.2113/gssajg.118.2.129, 2015.

823 Kubik, P.W. and Christl, M.: ^{10}Be and ^{26}Al measurements at the Zurich 6 MV Tandem AMS facility. *Nucl. Instrum. Methods*
824 *in Phys. Res. Section B*, 268, 880–883, doi: 10.1016/j.nimb.2009.10.054, 2010.

825 Lawson, A.C.: The epigene profiles of the desert. *Uni. California Dept. Geol. Bull.*, 9, 23–48, 1915.

826 Lidmar-Bergström, K.: Exhumed cretaceous landforms in south Sweden. *Z. Geomorph.: Supp. Band 72*, 21–40, 1988.

827 Lustig, L.K.: Trend surface analysis of the Basin and Range province, and some geomorphic implications. *US Geol. Surv.*
828 *Profess. Paper 500-D*, 1969.

829 Marker, M.E. and Holmes, P.J.: Laterisation on limestones of the Tertiary Wankoe Formation and its relationship to the African
830 Surface, southern Cape, South Africa. *Catena*, 38, 1-21, doi: 10.1016/S0341-8162(99)00066-1, 1999.

831 Marker ME, Holmes PJ. 2005. Landscape evolution and landscape sensitivity: the case of the southern Cape. *South African*
832 *Journal of Science*: 101, 53 - 60.

833 Marker, M.E., McFarlane, M.J. and Wormald, R.J.: A laterite profile near Albertinia, Southern Cape, South Africa: its
834 significance in the evolution of the African Surface. *S. Afr. J. Geol.*, 105, 67-74, doi: 10.2113/1050067, 2002.

835 Margerison, H.R., Phillips, W.M., Stuart, F.M. and Sugden, D.E.: Cosmogenic ^3He concentrations in ancient flood deposits
836 from the Coombs Hills, northern Dry Valleys, East Antarctica: interpreting exposure ages and erosion rates. *EPSL*, 230, 163-
837 175, doi: 10.1016/j.epsl.2004.11.007, 2005.

838 Midgley, G.F., Hannah, L., Millar, D., Thuiller, W. and Booth, A.: Developing regional and species-level assessments of
839 climate change impacts on biodiversity in the Cape Floristic Region. *Bio. Cons.*, 112, 87-97, doi: 10.1016/S0006-
840 3207(02)00414-7, 2003.

841 Moore, A., Blenkinsop, T. and Cotterill, F.W.: Southern African topography and erosion history: plumes or plate tectonics?
842 *Terra Nova*: 21, 310-315, doi: 10.1111/j.1365-3121.2009.00887.x, 2009.

843 Mountain, E.D: Grahamstown peneplain. *Trans. Geol. Soc. S Afr.*, 83, 47-53, 1980.

844 Norton, K.P. and Vanacker, V.: Effects of terrain smoothing on topographic shielding correction factors for cosmogenic
845 nuclide-derived estimates of basin-averaged denudation rates. *ESPL*, 34, 145-154, doi: 10.1002/esp.1700, 2009.

846 Nyblade, A.A. and Robinson, S.W.: The african superswell. *Geophys. Res. Lett.*, 21, 765-768, doi: 10.1029/94GL00631, 1994.

847 Ollier, C.: *Ancient landscapes*. Belhaven Press, London/New York, 233 pp, 1991.

848 Ollier, C. and Pain, C.: *The origin of mountains*. Routledge, London/New York, 345 pp, 2000.

849 Ouimet, W.B., Whipple, K.X., Crosby, B.T., Johnson, J.P. and Schildgen, T.F.: Epigenetic gorges in fluvial landscapes. *ESPL*,
850 33, 1993-2009, doi: 10.1002/esp.1650, 2008.

851 Owen, L.A., Finkel, R.C., Barnard, P.L., Haizhou, M., Asahi, K., Caffee, M.W. and Derbyshire, E.: Climatic and topographic
852 controls on the style and timing of Late Quaternary glaciation throughout Tibet and the Himalaya defined by ^{10}Be cosmogenic
853 radionuclide surface exposure dating. *Quat. Sci. Rev.*, 24, 1391-1411, doi: 10.1016/j.quascirev.2004.10.014, 2005.

854 Paige, S.: Rock-cut surfaces in the desert regions. *J. Geol.*, 20, 442–50, 1912.

855 Panario, D., Gutiérrez, O., Sánchez Bettucci, L., Peel, E., Oyhantçabal, P., Rabassa, J.: Ancient landscapes of Uruguay. In:
856 Rabassa, J. and Ollier, C. (Eds.) *Gondwana landscapes in southern South America*, pp. 161–199, 2014.

857 Parsons, A.J. and Abrahams, A.D.: Mountain mass denudation and piedmont formation in the Mojave and Sonoran Deserts.
858 *Am. J. Sci.*, 284, 255–71, 1984.

859 Partridge, T.C.: Cainozoic environmental change in southern Africa, with special emphasis on the last 200 000 years. *Prog.*
860 *Phys. Geog.*, 21, 3-22, doi: 10.1177/030913339702100102, 1997.

861 Partridge, T.C. 1998. Of diamonds, dinosaurs and diastrophism: 150 million years of landscape evolution in southern Africa.
862 *South African Journal of Geology*: 101, 165–184.

863 Partridge, T.C.: Evolution of Landscapes. In: Cowling, R.M., Richardson, D.M. and Pierce, S.M. (eds). *Vegetation of southern*
864 *Africa*. Cambridge University Press, pp. 1-20, 1999.

865 Partridge, T.C. and Maud, R.R.: Geomorphic evolution of southern Africa since the Mesozoic. *S. Afr. J. of Geol.*, 90, 179-
866 208, 1987.

867 Partridge, T.C. and Maud, R.R. Macro-scale geomorphic evolution of southern Africa. In Partridge T.C. and Maud, R.R.M.
868 (eds) *The Cenozoic of southern Africa*. Oxford University Press. pp. 3 – 18, 2000.

869 Paton, D.A.: Influence of crustal heterogeneity on normal fault dimensions and evolution: southern South Africa extensional
870 system. *J. Struct. Geol.*, 28, 868-886, doi: 10.1016/j.jsg.2006.01.006, 2006.

871 Peulvast, J.P. and Bétard F.: A history of basin inversion, scarp retreat and shallow denudation: The Araripe basin as a keystone
872 for understanding long-term landscape evolution in NE Brazil. *Geomorph.*, 233, 20-40, doi: 10.1016/j.geomorph.2014.10.009,
873 2015.

874 Portenga, E.W. and Bierman, P.R.: Understanding Earth's eroding surface with 10 Be. *GSA Today*: 21, 4-10, doi:
875 10.1130/G111A.1, 2011.

876 Rich, J.L.: Origin and evolution of rock fans and pediments. *Bull. Geol. Soc. Am.*, 46, 999–1024, doi: 10.1130/GSAB-46-999,
877 2935, 1935.

878 Richardson, J.C., Hodgson, D.M., Wilson, A., Carrivick, J.L. and Lang A.: Testing the applicability of morphometric
879 characterisation in discordant catchments to ancient landscapes: A case study from southern Africa. *Geomorph.*, 201, 162-176,
880 doi: 10.1016/j.geomorph.2016.02.026, 2016.

881 Richardson, J.C., Hodgson, D.M., Paton, D., Craven, B., Rawcliffe, A. and Lang, A.: Where is my sink? Reconstruction of
882 landscape development in southwestern Africa since the Late Jurassic. *Gondwana Res.*: 45, 43-64, doi:
883 10.1016/j.gr.2017.01.004, 2017.

884 Rogers, C.A.: The geological history of the Gouritz River system. *Trans. S. Afri. Phil. Soc.*, 14, 375-384, 1903.

885 Romans, B.W., Castellort, S., Covault, J.A., Fildani, A. and Walsh, J.P.: Environmental signal propagation in sedimentary
886 systems across timescales. *Earth-Sci. Rev.*: 153: 7-29, doi: 10.1016/j.earscirev.2015.07.012, 2016.

887 Ruzkiczay-Rüdiger, Z., Braucher, R., Csillag, G., Fodor, L.I., Dunai, T.J., Bada, G., Bourlés, D. and Müller, P.: Dating
888 Pleistocene aeolian landforms in Hungary, Central Europe, using in situ produced cosmogenic 10Be. *Quat. Geochron.*, 6, 515-
889 529, doi: 10.1016/j.quageo.2011.06.001, 2011.

890 Scharf, T.E., Codilean, A.T., de Wit, M., Jansen, J.D., Kubik, P.W.: Strong rocks sustain ancient postorogenic topography in
891 southern Africa. *Geol.*, 41, 331-334, doi: 10.1130/G33806.1, 2013.

892 Sharp, R.P.: Geomorphology of the Ruby–East Humboldt Range, Nevada. *Bull. Geol. Soc. Am.*, 51, 337–72, doi:
893 10.1130/GSAB-51-337, 1940.

894 Sømme, T.O., Piper, D.J., Deptuck, M.E. and Helland-Hansen, W.: Linking onshore–offshore sediment dispersal in the Golo
895 source-to-sink system (Corsica, France) during the Late Quaternary. *J. Sed. Res.*: 81, 118-137, doi: 10.2110/jsr.2011.11, 2011

896 Sonibare, W.A., Sippel, J., Scheck-Wenderoth, M. and Mikeš, D.: Crust-scale 3D model of the Western Bredasdorp Basin
897 (Southern South Africa): data-based insights from combined isostatic and 3D gravity modelling. *Basin Res.*, 27, 125-151, doi:
898 10.1111/bre.12064, 2015.

899 Spikings, A.L., Hodgson, D.M., Paton, D.A. and Spychala, Y.T.: Palinspastic restoration of an exhumed deep-water system:
900 a workflow to improve paleogeographic reconstructions. *Interpretation*, 3, SAA71-SAA87, doi: 10.1190/INT-2015-0015.1,
901 2015

902 Stanley, J.R., Braun, J., Baby, G., Guillocheau, F., Robin, C., Flowers, R.M., Brown, R., Wildman, M. and Beucher, R.:
903 Constraining plateau uplift in southern Africa by combining thermochronology, sediment flux, topography, and landscape
904 evolution modeling. *J. Geophys. Res.: Solid Earth*, 126(7), p.e2020JB021243, doi: 10.1029/2020JB021243, 2021

905 Summerfield, M.A.: Silcrete as a palaeoclimatic indicator: evidence from southern Africa. *Palaeo.*, *Palaeo.*, *Palaeo.*, 41, 65-
906 79, doi: 10.1016/0031-0182(83)90076-7, 1983.

907 Tankard, A., Welsink, H., Aukes, P., Newton, R. and Stettler, E.: Tectonic evolution of the Cape and Karoo basins of South
908 Africa. *Mar. Pet. Geol.*, 26, 1379-1412, doi: 10.1016/j.marpetgeo.2009.01.022, 2009.

909 Tinker, J., De Wit, M. and Brown, R.: Mesozoic exhumation of the southern Cape, South Africa, quantified using apatite
910 fission track thermochronology. *Tectonophys.*: 455, 77-93, doi: 10.1016/j.tecto.2007.10.009, 2008a.

911 Tinker J., de Wit, M. and Brown, R.: Linking source and sink: evaluating the balance between onshore erosion and offshore
912 sediment accumulation since Gondwana break-up, South Africa. *Tectonophys.*, 455, 94-103, doi: 10.1016/j.tecto.2007.11.040,
913 2008b.

914 Twidale, C.R.: *Ancient Australian Landscapes*. Rosenberg Pub Pty Limited, 144 pp, 2007a.

915 Twidale, C.R.: Bornhardts and associated fracture patterns. *Rev. As. Geol. Arg.*, 62, 139–153, 2007b.

916 Valetton, I.: Palaeoenvironment of lateritic bauxites with vertical and lateral differentiation. *Geol. Soc. London Sp. Pub.*, 11,
917 77–90, doi: 10.1144/GSL.SP.1983.011.01.10, 1983.

918 Vandermaelen, N., Beerten, K., Clapuyt, F., Christl, M. and Vanacker, V.: Constraining the aggradation mode of Pleistocene
919 river deposits based on cosmogenic radionuclide depth profiles and numerical modelling. *Geochronology*, 4, 713-730, doi:
920 10.5194/gchron-4-713-2022, 2022.

921 Vanacker V., von Blanckenburg, F., Hewawasam, T. and Kubik, P.W.: Constraining landscape development of the Sri Lankan
922 escarpment with cosmogenic nuclides in river sediment, *EPSL*, 253, 402-414, doi: 10.1016/j.epsl.2006.11.003, 2007.

923 Vanacker, V., von Blanckenburg, F., Govers, G., Molina, A., Campforts, B. and Kubik, P.W.: Transient river response,
924 captured by channel steepness and its concavity. *Geomorph.*, 228, 234-243, doi: 10.1016/j.geomorph.2014.09.013, 2015.

925 van der Beek, P., Summerfield, M.A., Braun, J., Brown, R.W. and Fleming A.: Modeling postbreakup landscape development
926 and denudational history across the southeast African (Drakensberg Escarpment) margin. *J. Geophys. Res.: Solid Earth*: 107
927 (B12), doi: 10.1029/2001JB000744, 2002.

928 van der Wateren, F.M. and Dunai, T.J.: Late Neogene passive margin denudation history—cosmogenic isotope measurements
929 from the central Namib desert. *Glob. and Planet. Change*, 30, 271-307, doi: 10.1016/S0921-8181(01)00104-7, 2001.

930 van Niekerk, H.S., Beukes, N.J. and Gutzmer, J.: Post-Gondwana pedogenic ferromanganese deposits, ancient soil profiles,
931 African land surfaces and palaeoclimatic change on the Highveld of South Africa. *J. Afr. Earth Sci.*, 29, 761-781, doi:
932 10.1016/S0899-5362(99)00128-1, 1999.

933 Vermeesch, P.: CosmoCalc: An Excel add-in for cosmogenic nuclide calculations. *Geochem., Geophys., Geosyst.*: 8,
934 doi:10.1029/2006GC001530, 2007

935 von Blanckenburg F., Belshaw, N. and O'Nions, R.: Separation of ^9Be and cosmogenic ^{10}Be from environmental materials
936 and SIMS isotope dilution analysis. *Chem. Geol.*, 129, 93–99, doi: 10.1016/0009-2541(95)00157-3, 1996.

937 von Blanckenburg, F., Hewawasam, T., Kubik, P.W.: Cosmogenic nuclide evidence for low weathering and denudation in the
938 wet, tropical highlands of Sri Lanka. *J. Geophys. Res.: Earth Surface*: 109, F3, doi: 10.1029/2003JF000049, 2004.

939 Widdowson, M.: Laterite and Ferricrete. In: Nash DJ, McLaren SJ. (eds.) *Geochemical Sediments and Landscapes*. Oxford,
940 UK: Wiley-Blackwell, pp. 46–94, 2007.

941 Wildman, M., Brown, R., Watkins, R., Carter, A., Gleadow, A. and Summerfield, M.: Post break-up tectonic inversion across
942 the southwestern cape of South Africa: new insights from apatite and zircon fission track thermochronometry. *Tectonophys.*,
943 654, 30–55, doi: 10.1016/j.tecto.2015.04.012, 2015.

944 Wildman, M., Brown, R., Beucher, R., Persano, C., Stuart, F., Gallagher, K., Schwanethal, J. and Carter, A.: The chronology
945 and tectonic style of landscape evolution along the elevated Atlantic continental margin of South Africa resolved by joint
946 apatite fission track and (U-Th-Sm)/He thermochronology. *Tectonics*: 35, doi: 10.1002/2015TC004042, 2016.

947 Wildman, M., Brown, R., Persano, C., Beucher, R., Stuart, F.M., Mackintosh, V., Gallagher, K., Schwanethal, J. and Carter,
948 A.: Contrasting Mesozoic evolution across the boundary between on and off craton regions of the South African plateau
949 inferred from apatite fission track and (U-Th-Sm)/He thermochronology. *J. Geophys. Res.: Solid Earth*, 122(2), pp.1517-1547,
950 doi: 10.1002/2016JB013478, 2017.

951 Willenbring, J.K. and von Blanckenburg, F.: Long-term stability of global erosion rates and weathering during late-Cenozoic
952 cooling. *Nature*: 465, 211-214, 2010.

953 Wittmann H., von Blanckenburg, F., Kruesmann, T., Norton, K.P. and Kubik, P.W.: Relation between rock uplift and
954 denudation from cosmogenic nuclides in river sediment in the Central Alps of Switzerland. *J. Geophys. Res.: Earth Surface*:
955 112 (F4), doi: 10.1029/2006JF000729, 2007.

956 Wittmann H., Von Blanckenburg, F., Guyot, J.L., Maurice, L., Kubik, P.W.: From source to sink: Preserving the cosmogenic
957 ^{10}Be -derived denudation rate signal of the Bolivian Andes in sediment of the Beni and Mamoré foreland basins. *EPSL*, 288,
958 463-474, doi: 10.1016/j.epsl.2009.10.008, 2009.
959
960
961